PORATBLE, CONFIGURABLE IMPEDANCE MEASUREMENT DEVICE FOR SWEAT BASED GLUCOSE DETECTION

by

Athul Asokan Thulasi

APPROVED BY SUPERVISORY COMMITTEE:

Dr. Dinesh K Bhatia, Chair

Dr. Poras Balsara

Dr. Shalini Prasad

Dedicated to my parents, Asokan and Thulasi

PORATBLE, CONFIGURABLE IMPEDANCE MEASUREMENT DEVICE FOR SWEAT BASED GLUCOSE DETECTION

by

ATHUL ASOKAN THULASI, B.Tech

THESIS

Presented to the Faculty of

The University of Texas at Dallas

in Partial Fulfillment

of the Requirements

for the Degree of

MASTER OF SCIENCE IN

ELECTRICAL ENGINEERING

THE UNIVERSITY OF TEXAS AT DALLAS

May 2017

ACKNOWLEDGMENTS

First and foremost, I would like to thank Dr. Dinesh K Bhatia for inspiring me to pursue a thesis and allowing me to be a part of IDEA lab. I am grateful to him for believing in me, supporting me, encouraging me, providing feedback and direction throughout the course of my thesis. I would not have even considered pursuing a thesis, if he hasnt offered to take me in as his student. I am extremely happy that I chose to do thesis under his guidance. I also thank him for patience, understanding and time he has spent for helping me complete the thesis.

Second, I would like to thank other members of my committee Dr. Poras Balsara and Dr. Shalini Prasad for their guidance and support. The suggestions and feedback given by Dr Balsara during our lab meetings were very valuable for my thesis. I am grateful to Dr. Prasad for giving me access to work with the glucose sensors developed in the Biomedical Microdevices and Nanomaterials Lab(BMNL) and providing me guidance through her student Dr. Munje Rujuta.

Third, I would like to thank Dr. Munje Rujuta, for her dissertation work on a flexible non-porous double layer electrochemical biosensor for glucose detection gave my thesis a purpose. I am indebted to her for the initial dataset which helped me get started with my work. I am also thankful for her help in understanding the sensor and for making sensor samples for me to test. I would like to thank Badrinath, Ambalika and Akshay from BMNL lab who had spared some of their time to help me.

Next, I would like to thank my lab members Devang, Abhishek, Rohit, Sameer, Sharath and Girish for their suggestions. They have given me ideas and helped me solve problems that I faced during the thesis work.

Next, I would like to thank Analog Devices Inc. and Linear Technology Corporation for providing me samples of the integrated circuit parts that were required to build the designed device. My thesis would not be complete without their samples.

Next, I would like to thank my friends, Goutham Ravindran and Rithunraj Krishna who always listened to me and kept me motivated till the completion of the thesis.
Finally, I would like to thank my family who always encouraged me and prayed to god for his blessings.

December 2016

PORATBLE, CONFIGURABLE IMPEDANCE MEASUREMENT DEVICE FOR SWEAT BASED GLUCOSE DETECTION

Athul Asokan Thulasi, MS
The University of Texas at Dallas, 2017

Supervising Professor: Dr. Dinesh K Bhatia, Chair

The future of disease diagnostics lies in the development of low-cost sensors that can detect minute traces of pathogens or antigens from body fluids. Developments in nanotechnology and biomedical research have already shown us that a nanosensor can be specifically tailored to detect a specific biomolecule. These sensors would allow patients to run point of care diagnostic tests, thereby saving time and cost of running clinical tests and can give early stage disease diagnosis and help physicians to provide personalized treatment. This work involves the development of a configurable electronic sensor platform that will interface with these sensors. The device is tested by quantification of glucose from sweat using a nanosensor developed in the Biomedical Microdevices and Nanotechnology Lab in the University of Texas at Dallas. The platform can be easily configured to run Electrochemical Impedance Spectroscopy based detection test for other biomolecules by using sensor tailored for it.

TABLE OF CONTENTS

LIST OF FIGURES

LIST OF TABLES

CHAPTER 1

INTRODUCTION

The future of disease diagnostics lies in the development of low-cost sensors that can detect minute traces of antigens produced by pathogens or antibodies produced by body; from body fluids like sweat, saliva, tear, blood etc. Antigens are generally proteins produced by a pathogen that are foreign to the immune system of a person, and it causes an immune response. The body produces antibody in response to the antigen to fight them. Presence of disease causing pathogens can be confirmed by identifying and quantifying antigens produced by them or by identifying and quantifying the antibodies produced by the body. Therefore, detecting and quantifying these biomolecules can be used for disease diagnosis. The presence of these antigens or antibodies above a threshold is an indication of disease. Developments in nanotechnology and biomedical research have already shown us that a nanosensor can be tailored to detect a specific biomolecule [1][4][5]. It is only a matter of time that these sensors would become cheap, accurate and early stage diagnosis tools for detecting disease. Once this sensor technology becomes robust, disease diagnosis for common diseases would become quick point of care test like the strip based blood glucose test for diabetes that exists in present day. By enabling patients to run point of care diagnostic tests, these sensors would save time and cost of running clinical tests and can give early stage detection of their condition. It could also help physicians to provide personalized and dynamically tailored treatment per the exact severity of their patients medical condition. An added advantage is the elimination of error due to mismanagement of test samples in a clinical test laboratory. Disease diagnosis using this type of tests also has the potential to evolve a new class of continuous health monitoring device that can assist in diagnosis of common ailments. These tests can detect symptoms of a disease in a very early stage. Indicators for common ailment can become a continuous monitoring parameter like heart rate, blood pressure or temperature that exists in present day health monitoring devices.

1.1 The missing piece in the solution

There exists a need for a low cost, portable (or wearable) device that can be used for disease diagnosis that could interface with the sensors and can detect and quantify the antigens or antibodies present in body fluids. It would be ideal to have a single device that can interface with any sensor that belongs to this class. The portability and low cost feature is very important design requirement as this is a health care device and hence is supposed to be accessible to all geographic regions and affordable to economic classes.

The main issue that exists in developing such a measurement device is that there exit a multitude of measurement techniques that can be used to detect and quantify the antigen depending on the characteristics of the antigen. The sensing technique could involve exploiting the antigen-antibody response to light or magnetic field or electric field (electrochemical techniques) and translating it to an electrically measurable quantity. The method that works best for one antigen may not work well for another. The best technique for any antigen can only be decided by studying and experimenting with the antigen-antibody response to various sensing techniques. Due to the existence of myriad of sensing techniques there exist a large design variety of sensor-measurement device interfaces. One device that can accommodate the entire range of sensor-measurement device interfaces is not feasible to be constructed as a portable device.

Accommodating all techniques into a single measurement would also result in a large design in terms of size and power consumption, rendering it as non-portable and costly equipment. The design requirements of the ideal device are to be low power and be battery powered, to be low footprint and be wearable, to be low cost and be accessible to all economic classes, to be able to interface to all sensing techniques, and to be able support all measurement techniques. This is however not practical as former three requirements contrast with the latter two requirements.

The two extreme designs solutions would be to, either have a design that supports one technique and one sensor-measurement device interface that is low cost, low power, low footprint or have a design that supports all known techniques and sensor interfaces which will consume more power, have large footprint and be costlier. The former extreme design case is relatively more useful than the latter case. The former design is useful for single antibody detection (even though it requires huge design effort to scale to other antibodies and cost of having different test is still high) and latter is not really feasible to be a portable, low cost device. We would hence, like to be closer to the first extreme design case in a practical scenario.

1.2 Cost effective incorporation of multiple techniques in a single device

It is not possible to have a single piece of hardware that can come close to the ideal solution. However, we could capitalize on the fact that all tests need not be run simultaneously. The solution to making the design incorporate many measurement techniques and remain close to the low power, low cost, low footprint side of the design space is to modularize the design into two different physical parts with a standard interface between them. One part which is fixed for all measurements should be relatively low cost, low foot, low power consumption part which can be easily configured to support one among all the sensing techniques at a time. By supporting only one measurement at a time this part can be far less complicated and have lower cost, lower power consumption, and lower foot print when compared to the latter extreme design case. Let us call this part as the fixed configurable module (FCM). It is a fixed hardware for all diagnosis tests and should be configurable (hardware and/or software) to suit any sensing technique. The second part could be very low power, very low footprint and very low cost part having specific interface for one type of sensor. It is the part that would change based on the sensing technique. Let us call this part as technique specific reusable module (TSRM). The module is called reusable to indicate that it can be

reused for multiple runs of the diagnosis test and is not a one-time use part. The sensors that attach to this module can be either one time use or reusable. The TSRM is not specific to a disease or sensor but is specific to a sensing technique. If there are multiple diseases that could be detected using the same technique but with different sensors, then the same TSRM module can be reused. The Electrochemical Impedance Spectroscopy (EIS) is an example of a technique that can be used to detect multiple different biomolecules. It can be used to detect glucose from sweat [1][4] and it can be used to detect lactic acid [2]. The technique specific reusable module (TSRM) should be able to attach to the fixed configurable module (FCM) through a standard interface as we should be able to swap TSRM module to run a different test. The interface between TSRM and the sensor can be a specific interface for each sensor but it is better to have a standard interface if there exist one for a specific sensing technique.

The modular design dictates that the functions of the entire measurement device to be partitioned into two parts. The measurement device functions can be classified as user input, configuration of the system, analog sensing, calibration of the device, computation of results and display of results. The functions like user input, display of result can be easily assigned to the fixed configurable module (FCM) because the hardware required for it can be constant for any measurement technique. Some of these functions can also be done using a smartphone application that connects to the FCM as smartphones are becoming ubiquitous [2]. The front-end interface to the sensor for sensing should be assigned to the technique specific reusable module (TSRM) as the hardware requirement for it can be different for measurement techniques. The functions like configuration, calibration and computation of results can be in either of the modules as these are specific to the sensing technique and hence be in the TSRM but it can also be implemented using a microcontroller which can be reprogrammed by a host or by a reconfigurable device like a field programmable gate array (FPGA). The choice of where these functions are to be allocated depends on factors like

required accuracy and precision, cost, power and must be decided on a case by case basis. It is preferable to have most of these functions to in the fixed configurable module (FCM) to make the technique specific reusable module (TSRM) relatively simple and low cost.
The interconnect between the two types of modules must be standard interface because the technique specific reusable module (TSRM) should be replaced with a different technique specific reusable module (TSRM) to be able to use a different measurement technique. A fixed low speed bus like I2C (Inter IC Communication) or SPI (Serial Peripheral Bus) would suffice the requirement if the fixed configurable module (FCM) as it can simultaneously handle multiple sensors connected to it. Another alternative would be to use a packet switched interconnection network if there is large number variety of sensors that it must handle. The vision of the final product that could emerge out of this research and its successors would be a system that consists of a wearable FCM module that connects wirelessly to several tiny TSRM patches attached to different parts of body through very low power interface like ZigBee or Bluetooth Low Energy. It would monitor body fluids to have a real-time disease diagnosis and health monitoring. The FCM can also be designed to connect to TSRM through conductive fabric designed by google ATAPs project jacquard [9]. The FCM module would connect to a smartphone via Bluetooth or connect to a Wi-Fi hotspot to configure itself for the required diagnosis test.

1.2.1 Scope of the work

The thesis work presented here details the development of a modular electronic sensor platform that can be configured to work with any biosensor that works on two electrode impedance spectroscopy. This device is developed as a proof of concept and tested by detection and quantification of glucose (antigen) from sweat using a nanosensor developed in the Biomedical Microdevices and Nanotechnology Lab (BMNL) at the University of Texas at Dallas [1]. The sensor works using two electrode Electrochemical Impedance Spectroscopy

(EIS) as a measurement technique on the sweat sample placed on the sensor. Even though glucose is not produced by any pathogen, glucose present in sweat is considered an antigen in the rest of this manuscript because, excessive quantity indicates that the human pancreas is unable to produce enough insulin (diabetes); hence it can be considered an antigen in the sense that it is indicative of a disease.

Here, Electrochemical Impedance spectroscopy (EIS) as the name suggests involves finding the impedance of the sensor in a range of frequencies for varying concentrations of glucose. The frequency that shows maximum observable change in impedance for even slight change in the glucose concentration is identified. This frequency is influenced by the sensor chemistry and the antibody-antigen interaction [1][4]. Impedance measurements are then, done in this identified fixed frequency to find out a correlation between the measured impedance difference from baseline sensor versus concentration of glucose by application of known concentration of glucose. Once this correlation is discovered then the reusable part of the measurement device (TSRM) can be designed to the specifications required to measure impedance in the range seen during the correlation studies. The correlation can be expressed as a look up table or a curve fitting equation. This is programmed to the fixed configurable module (FCM) and is used to find out the concentration of the glucose for a sample with unknown concentration of glucose. The sweat glucose thresholds can be then used to determine if the measurement is a positive/negative for diabetes. The platform can be easily extended to run EIS based detection test for other biomolecules by replacing the sensor to a different sensor tailored for the biomolecule under test and configuring the fixed configurable module (FCM) with new set of correlation look up table. The device can be extended to other sensing techniques with development of specific technique specific reusable module (TSRM)s to those techniques. This work only includes the development of technique specific reusable module (TSRM) for two electrode EIS based sensing technique for biomolecules. This platform along with already existing activity monitoring devices could

enable researchers to conduct studies on patients with a disease the without interfering their normal lifestyle. This would allow studying a larger set of patients and give more accurate results to study the effect of lifestyle. This could lead to development of lifestyle related disease diagnosis and development of more accurate bio sensors and measurement devices.

1.3 Literature survey

This section goes briefly explains few of the work done by researchers that aligns with this work. It includes the works relating to instrumentation required for Electrochemical Impedance spectroscopy and other measurement techniques that are intended for quantifying biomolecules present in human body. Majority of this chapter deals with works that implemented impedance measurement using AD5933 (High performance Impedance Converter Network) from Analog Devices.

1.3.1 Smartphone as a diagnostic assistant device

Alexander Sun et al. [3] had built a prototype design for a reconfigurable potentiostat that supports multiple measurement techniques. The device has an analog front end that can be configured to support Amperometry, potentiometry and impedance spectroscopy. It was used to measure pH and perform a glucose assay. The design is made up of a microcontroller that interfaces with the analog front end with a four channel ADC and four channel DAC and communicates to a host device like a smartphone using serial communication. They presented the idea of using smartphone and biosensors to extract heath related parameters that can be used for remote or at-home diagnosis tests. Their prototype system was not in the size requirement to be integrated to a smartphone device, however it showed that multiple molecular biosensor based measuring techniques can be integrated into a design.

1.3.2 Blood glucose measurement using bio-impedance technique

D.K Kamat et al. [22] have built a bio impedance monitor using AD5933 and LPC1768 microcontroller for measurement of glucose in blood using silver electrodes as body contacts. Radio wave transmission through body and determining the signal attenuation, photo plethysmography are some other techniques used in determining blood glucose levels. These techniques have drawbacks due to use of high frequency radio waves and requirement of additional sensor for detecting heart rhythm respectively. The body impedance and its dependence on glucose concentration was studied by measuring impedance using the developed device and performing invasive measurements of glucose concentration using ACCU-CHECK glucose meter. It is seen that impedance decreases with increase in blood glucose level and vice versa. 10 KHz to 100KHz was the chosen frequency for the measurement as these frequencies yielded larger change in impedance for a given change in glucose concentration.

1.3.3 Impedance measurement for corrosion studies

Jenzy Hoja, Grzegorz Lentka [19] had built a impedance measurement device using two AD5933 chips and a AT32UC3B1256 microcontroller designed from in-field corrosion studies. They used two AD5933 chips in their system instead of using one and eliminated the need for calibrating the device before measurement of impedance. One of it was used to measure the orthogonal component of current flowing through the impedance and the other one was used to measure the orthogonal component of the voltage signal applied across the impedance. The use of two AD5933 required a work around the problem of having same I2C address for both AD5933 devices. The devices had to operate synchronously for the measurement to give meaningful result. Two I2C buses were emulated on the same port of the microcontroller to overcome the address conflict and need for synchronous operation. An external signal conditioning circuit was used to extend the measurement frequency from (1KHz to 100KHz) to (0.1Hz to 100KHz) and the impedance range to (100 Ohm to 10G Ohm). The range of

impedance that was measured was increase using a selectable resistor in parallel with the measured impedance. An error correction formula was required to remove the error caused by the external signal conditioning circuitry. The relative error in magnitude of impedance was reported to be +/- 1.6

1.3.4 Impedance meter used for biosensor application

Konard Chabowski et al. [10] built an impedance measurement device for microbiology related impedance sensors using an AD5933 and ATmega32 microcontroller. The signal applied to the sensor must be low amplitude to prevent electrolysis of the biomolecules. The signal generated by AD5933 is attenuated by a constant factor of 10 before applying to the sensor. A DC bias canceller was implemented to avoid DC polarization of measured impedance. These are the two constraints on impedance measurement systems used for biomolecular impedance measurement. They have experimentally determined that the minimum input voltage required by the ADC internal to AD5933 to give an accurate result after single point DFT is 15mV. This determines the higher limit of impedance that the measurement system can measure with any gain setting resistor. AD5933 has a single point 1024 sample DFT core which samples at the master clock divided by a factor of 16 and a DDS core that generates sinusoids signal samples at 4 master clock cycles. They explained the need for the generated signal period over a 1024 sample period to be an integer to avoid errors due to leakage. If it cannot be an integer, then large number of output signal must be included in the 1024 sample time to reduce the effect of spectrum leakage.

1.3.5 Multiple metabolites and ions measured from sweat

Sweat is complex solution as it contains multiple metabolites and ions. Simultaneous and real time screening of multiple biomolecules is critical in generating useful physiological data. Wei Gao et al.[25] built a flexible wearable system that measures sweat metabolites

like glucose and lactate electrolytes like sodium and potassium ion. Skin temperature is also measured to calibrate the response of the sensors. They used a flexible sensor array for simultaneous and selective screening of panel of biomarker in sweat. The system consisted of separate analog front end for each sensor and a common microcontroller to configure and control the front end. Amperometry and potentiometry were used as sensing techniques. The developed wearable is used to measure the detailed sweat profile of human subjects engaged in prolonged physical activities. Real time sample collection and analysis is done using the device. Excessive loss of potassium and sodium in sweat could indicate dehydration or muscle cramps or hyponatremia or hypokalemia. Sweat glucose is related to blood glucose and hence can be used in diabetes detection. Sweat lactate can be potentially serve as marker for pressure ischemia. Skin temperature is useful to compensate other measurements and serves as a useful clinical parameter.

1.4 Contributions

The main contributions of this work include

- The development of a portable device that can measure glucose from sweat to avoid taking blood samples regularly for diabetes testing. This works with the sensor developed by [4].

- The architecture for a portable universal sensing platform for disease diagnosis validated using glucose measurement from sweat using electrochemical impedance spectroscopy.

- Reduced the size of measurement device from a CPU size box to a credit card size board.

1.5 Organization of thesis

The thesis is organized as follows

- Chapter 2 goes through the basics regarding the working of glucose sensor and comes up with the specific requirements of the system to detect glucose from sweat and to extend it to other electrochemical impedance sensor based techniques.
- Chapter 3 goes though the specifications, theory of working and the design of the technique specific reusable module and configuration of fixed configurable module in the use case of glucose detection from sweat.
- Chapter 4 goes through the final PCB design and its characterization.
- Chapter 5 details the testing results using the PCB board. It shows the functionality of the board and compares it with measurement made using Gamry 600 reference measurement device and digital multimeter.
- Chapter 6 includes concluding remarks and results. It also explores future scope of the work

CHAPTER 2

SENSOR BASICS AND SYSTEM SPECIFICATIONS

This describes the basics concepts and background study required to understand the work done as part of this thesis. It explains the relevance and advantage of using sweat based glucose detection. After that, it explains the basic functioning of sweat glucose sensor for which the TSRM is designed and then it comes up with the specifications of the design.

2.1 Is sweat glucose level relevant?

The primarily consideration before designing a sweat based glucose detection device is to consider the validity of glucose present in sweat as a useful parameter to identify diabetes. There are two aspects to the validity of sweat glucose for diabetes studies. Sweat glucose concentration should be directly related to blood glucose concentration and availability of sweat for test. We should be able to obtain sweat when the test is to be done or wait for sweat to be produced to do the test. J. Moyer et al. [2] could study the correlation between blood glucose and sweat glucose and show that sweat glucose concentration is directly proportional to blood glucose concentration when the sweat is harvested using proper techniques that avoid contamination of sweat sample. They have simulated sweat using iontophoretic delivery of pilocarpine wherein they apply a current of 1mA for 10 minutes to the site where sweat is sampled. They showed that the sweat concentration is an order less in concentration when compared to blood glucose. The exact ratio varies from person to person and is dependent on the location of body from which the sweat is being sampled [2][26]. They measured the blood glucose concentration from 150mg/dl to 350mg/dL the sweat glucose from 1.5mg/dl to 4mg/dl for a person as shown in Figure 2.1 (which is an approximate version redrawn from [2]). The maximum range of glucose in human body reported in literature is from 1mg/dL to 100mg/dL [2][4][26]. The normal value of sweat glucose present is 5mg/dl to 20mg/dl

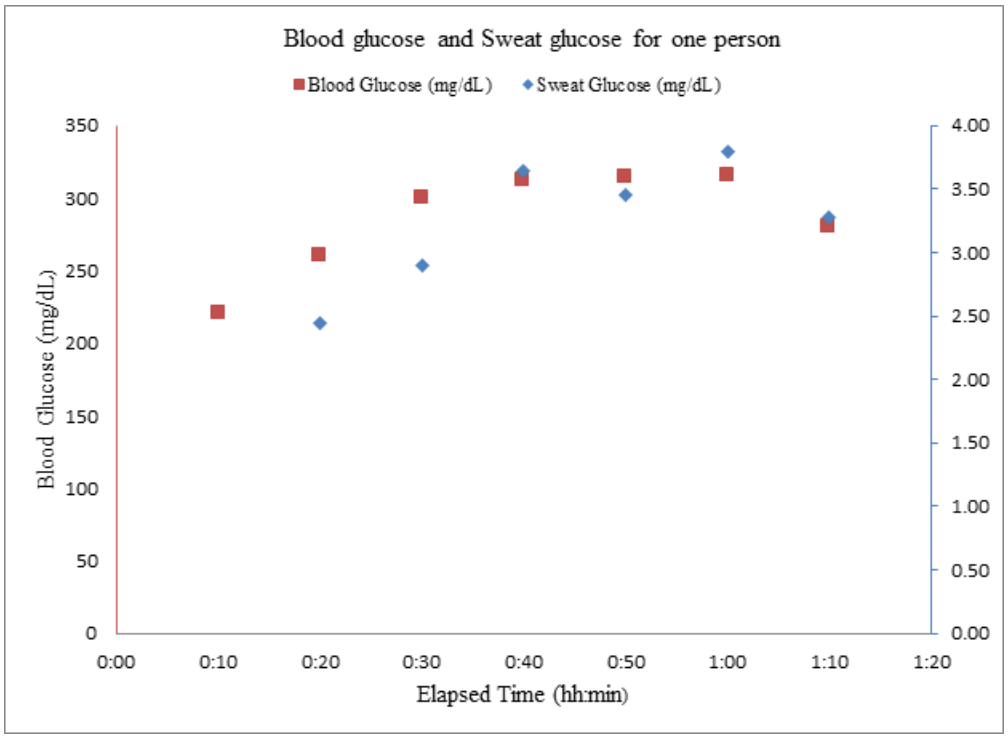

Figure 2.1. Approximated sweat glucose (diamonds) and blood glucose (squares) data for one subject in [2].

[26]. Their study also showed that the sweat glucose lags the blood glucose by around eight minutes [2]. They also have calculated the blood glucose level from the measurement of sweat glucose level and verifying it with a blood glucose measurement. They could predict the blood glucose level using the sweat glucose level. Even though the predicted blood glucose level from sweat glucose level is not always one hundred percent accurate, it gives close estimation of blood glucose with added advantage of being non-invasive. Current diabetes tests rely on blood glucose level to determine diabetes. Since the study shows that sweat glucose is has good correlation to blood glucose even though with a small lag in time, it could be used for diabetes studies if we calibrate the sweat glucose based on blood glucose level of a person.

2.2 How to quantify sweat glucose level?

There are several techniques that exist in literature that can be used to quantify sweat glucose concentration. Some of the techniques used include high performance liquid chromatography with pulsed amperometry detection (HPAE-PAD) [2], Electrochemical Impedance spectroscopy (EIS) [1], Chronoamperometry [3] and ionotophoresis of transdermal interstitial fluids and so on. This work limits its scope to Electrochemical Impedance Spectroscopy because the TSRM module was designed specifically for a sensor that works based on this technique and it is the most common method used in commercially available handheld glucose devices [4].

2.2.1 Electrochemical impedance spectroscopy (EIS)

Electrochemical Impedance spectroscopy is the technique that is used in majority of the commercially available handheld glucose biosensor in the market [4]. Impedance spectroscopy as the name suggest involves finding the impedance response of a system in a spectrum of frequency. The most common way of doing this is by exciting the system with sinusoids in the required frequency range of interest and applying a Digital Fourier Transform (DFT) to obtain the frequency response of the response of the system. Generally, the input signal is a sinusoidal voltage signal and the response is a current signal. It is hence possible to calculate the value of a complex impedance of a system using Impedance spectroscopy. The ratio of the input to the output gives the magnitude of impedance. The phase difference between the input and output signal is the phase difference of impedance. This process is repeated by scanning the frequency range required to obtain the impedance spectrum. When spectroscopy, the technique that is applied to an electrochemical system, it is termed as Electrochemical Impedance spectroscopy.

In an electrochemical system, the impedance response of the system is mainly influenced by

the formation of an electrical double layer (EDL) capacitor at the electrode-electrolyte interface and the amount charge transfer that occurs (represented by a charge transfer resistance) due to chemical reactions (usually redox reactions). An electrical double layer is created at the fluid electrode interface when an array of charged particles or oriented dipoles is present at the interface. The EDL capacitance value is dependent upon the surface chemistry of the electrode-electrolyte interface. The surface chemistry is affected by the concentration of the electrolyte that binds to the electrode surface due to chemical interactions and electrostatic interactions that happen in the system. This implies that the concentration of electrolyte translates into corresponding EDL capacitance and hence can be measured as an imaginary part of the impedance. The higher concentration of electrolyte creates a larger EDL capacitance and hence the imaginary part of the impedance will lower for higher concentrations. The amount of redox reaction that occurs is dependent on the concentration of the electrolyte under test if it participates in redox reactions that occur in the system. The real part of impedance decrease due to the free electrons generated by the redox reaction.

2.2.2 Electrical double layer formation

Electrical double layer is the structure that appears on the surface of solid object when it comes in contact to a fluid that contains charged particles and oriented dipoles as shown in figure 2.2. Two parallel layers of charge surrounding the solid object are formed constituting the electrical double layer. The inner layer of charge (closer to the solid object) is formed due to the ions absorbed to the solid due to the chemical interactions. This layer is called the inner Helmholtz plane (IHP) [6]. The outer layer is loosely attached with the solid layer and is formed due to columbic forces between the first layer and freely moving ions in the fluid that move under the influence of electric fields and thermal motion. This layer is called the outer Helmholtz plane (OHP) [6].

A simple electrical double layer is modeled as its equivalent Randels circuit shown in figure

2.2. The circuit consists of four elements. The uncompensated solution resistance (Rs) is the resistance offered by the fluid, electrical double layer capacitance (Cd) is capacitance due to formation of double layer, Polarization resistance (Rp) is the barrier resistance formed between the electrode and fluid and the Warburg impedance (Zw) which depends on the mass transport of reactant and product. The principal idea behind measuring glucose from sweat is that; if a senor can specifically bind and react to glucose then, the impedance change due to formation of electrical double layer and chemical reactions is dependent on value on the concentration of glucose in sweat. There is a decrease in impedance when a sweat sample containing glucose is added on the electrolytic sensor and the change in impedance will have a correlation to glucose concentration. The impedance difference from baseline (sensor with buffer solution and synthetic sweat) to that of sensor with sweat solution with glucose can be used to determine the glucose concentration in a sweat sample with unknown glucose concentration.

2.3 Basics of sensor construction and working

The objective of the sensor design is to be specific to glucose and give large impedance change even for a small change in sweat glucose concentration using small quantity of sweat. The sensor used to test the impedance measurement device is developed by Rujuta et al. [1] [4] in Biomedical devices and Nanotechnology Laboratory (BMNL) at the University of Texas at Dallas. The reaction that takes place between sweat glucose at the sensor is

$$Glucose + O_2 \xrightarrow[oxidation]{glucoseoxidase} D - glucono - 1,5 - lactone + H_2O_2$$

$$H_2O_2 \longrightarrow 2H^+ + O_2 + 2e^-$$

The sensor is made up of layers of materials staked on top of each other. The base material is made up of flexible Nano porous polyimide substrate which looks like paper. The electrode

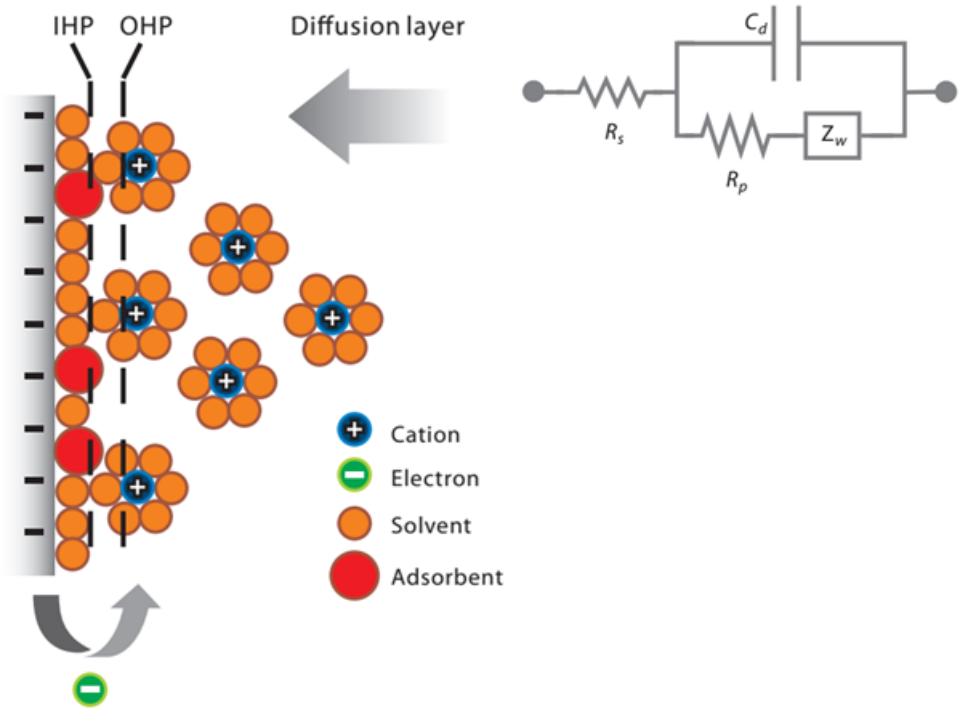

Figure 2.2. Approximated sweat glucose (diamonds) and blood glucose (squares) data for one subject in [2].

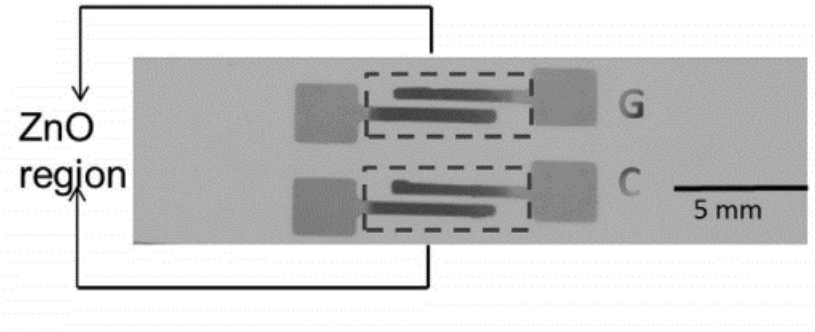

Figure 2.3. The glucose sensor used to test the TSRM [4].

and contact area is made of gold and the electrode area is spluttered with Zinc Oxide between the electrodes which form the two layers above the base material [4].

There several more layers stacked up to constitute the immunoassay for glucose. The layers include a linker layer, Glucose oxidase antibody, Glucose Oxidase enzyme. The glucose oxidase and glucose oxidase. These layers make the sensor specific to glucose. The

sensor was studied at various frequencies and the frequency gave the maximum detectable change in impedance was selected as the operating frequency of the sensor. This frequency was chosen as 100Hz [4]. The concentrations of sweat glucose from 10ug/ml (1mg/dl) to 1000ug/ml (100mg/dl) are of interest as it is the range that is reported to be present in human sweat. The change in impedance for known concentrations of glucose was further studied with a 100Hz input sinusoid and the average results were shown in Table 2.1. The results of the further studies were then used to determine a curve fitting function that can be used to determine glucose concentration from impedance difference. The study also gave a curve fitted equation for calculating glucose concentration from the percentage change in impedance from baseline. The TSRM module uses this fitting function that determines glucose concentration. The curve fitting function that was reported in [4] and has $R^2 = 0.9891$.

$$y = 31.7 + 2.55 * ln(x - 0.01)$$

Where, x is the sweat glucose concentration in mg/dl and y is the percentage change in impedance from baseline in Ohms. The value of R2 is an indicator of the effectiveness of the fitting function. It can lie between 0 and 1 and higher value indicates more effective fitting for the data. The sensor has a limit of detection of 0.01ug/ml and gets saturated above 1000ug/ml concentration of sweat glucose. The studies were done with a constant volume of synthetic sweat volume of 3 microliters. The concentration of glucose can be obtained from this curve fitting equation as

$$x = 0.01 + e^{\left(\frac{y-31.7}{2.55}\right)}$$

The glucose concentration in sweat can be measured by measuring the sensor baseline impedance (sensor and synthetic sweat with no glucose) followed by measuring the impedance of the sensor after adding 3 microliters of sweat sample containing glucose. There is need

Table 2.1. Average impedance change and its standard deviation for various concentration of glucose.

Average / (ug/mL)	**Baseline**	**0.01**	**1.00**	**10.00**	**100.00**	**1000.00**	**2000.00**
Impedance at 100 Hz	18289.16	15195.68	13508.40	12754.29	11772.57	10233.12	10686.82
Change from Baseline (%)		17%	26%	30%	36%	44%	42%
Standard deviation	1284.06	1356.34	1295.54	1298.08	1821.04	943.59	893.98
Standard deviation (%)	7%	9%	10%	10%	15%	9%	8%
Standard Error of Mean	4%	4%	5%	5%	8%	5%	4%
Max percentage change		21%	31%	35%	43%	49%	46%
Min percentage change		13%	21%	25%	28%	39%	38%

Note: The data provided in this table is the courtesy of Dr. Rujuta, Dr. Shalini Prasad et al. [1][4] from BMNL Lab at UT Dallas (private communication). The max and min percentage change can be used as a look up table to identify the concentration of glucose.

for waiting for an incubation time of 15 minutes before the impedance is measured after adding sweat sample containing unknown concentration of glucose. The percentage change in the impedance from the baseline can be calculated and used in the curve fitted equation to obtain the approximate value of the glucose concentration present in sweat. The curve fitted has equation has an error associated with it hence the calculated value also will have the same error. It will hence be able to calculate that the glucose concentration only accurate to a range of values.

An alternate method of calculating the concentration range is to use a look up table mapping glucose concentration to percentage change in impedance as show in table 2.1 (Max and Min percentage change). There is an overlap in the range of percentage impedance change for adjacent concentration ranges. The overlap implies that the sensor will not be able to calculate the glucose concentration to a single decade range, but calculate the upper and lower bound of the glucose concentrations to the nearest decade ranges.

2.4 System design requirements of the TSRM module

The impedance change studies over a range of frequency was used to determine that 50 to 200Hz input sinusoid has to be applied to the sensor to get a impedance change that is directly related to the concentration of the sweat glucose. Further studies were done at 100

Hz to find out the curve fitting equation that can be used to calculate the concentration of sweat glucose from measured change in impedance. All the measured impedances were in the range 8K Ohm to 20 K Ohm and hence the designed TSRM should be able to measure impedance in this range with accuracy.

The difference in impedance between 1ug/mL and 10ug/mL is the smallest impedance difference for a decade of change in glucose concentration among the decade pairs of concentration ranges that is present in the human sweat. The smallest impedance difference between these decade pairs is 754.11 Ohms (13508.40 Ohm 12754.29 Ohm from Table 1). This requires that for accurate detection of this decade range of the glucose the TSRM should at the least be able to accurately measure an impedance change of at least 375Ohm (half of the 754.11 Ohms). Another system requirement that is not obvious from the data presented here is that the TSRM should be able to generate low amplitude sinusoids mainly due to two reasons. First, the signal is applied to a biomolecule and high voltages and currents could damage the structure of the molecule. Second, the response of the sensor is non-linear for large inputs and hence to get an approximate linear response only a small amplitude signal can be applied to the sensor. The signal also cannot be too low as to make instrumentation impossible. 10mV RMS sinusoids have been used to study the sensor [1][4] and hence the designed TSRM should be able to generate signals as low as 10mV RMS.

CHAPTER 3

SYSTEM DESIGN

This chapter details the design of the system that would be used to measure glucose from sweat from the system specifications discussed in chapter 2. It explains the architecture of the designed system and functionality of its components. This includes the circuit design of the TSRM and configuration of FCM module to calculate impedance of the glucose sensor. It also explains the theory of the working of the system from an electrical circuit point of view.

The minimum system requirements of the TSRM module as described in chapter 2 is that it should be able to generate 10mV RMS sinusoid of 100 Hz frequency and measure the resulting current flowing through the test impedance which could be in the range of 8K Ohm to 20K Ohm. In addition to the minimum requirement, it should also be configurable to measure impedances in a different impedance range to be able to work with other sensors that work on the principle of Electrochemical Impedance spectroscopy (EIS). This implies that the module should be able to generate sinusoids of different amplitude and frequency. The FCM module should be able to configure the TRSM to generate sinusoids for different measurements requirements and do the impedance calculations. It should also handle any required user input, calculations required and display of results of the measurement.

The TSRM should be able to generate sinusoids of different frequency and amplitude and measure currents and report it back to the FCM through a standard interface. The FCM would use this information to calculate the impedance and the concentration of glucose or any other relevant parameter. The sensor should give an impedance that has some correlation with the quantity that we intend to measure (here concentration of glucose in sweat). The first task is to identify and implement methods to generate sinusoids which can vary amplitude and frequency. Once this done, implementation of circuit that would measure the current that flows through the sensor can be done.The impedance can be calculated from this

instrumentation. Depending on the requirements of the TSRM, an FCM system that can configure the TSRM can be designed which is flexible to be reprogrammed or reconfigured to suit other EIS based measurements.

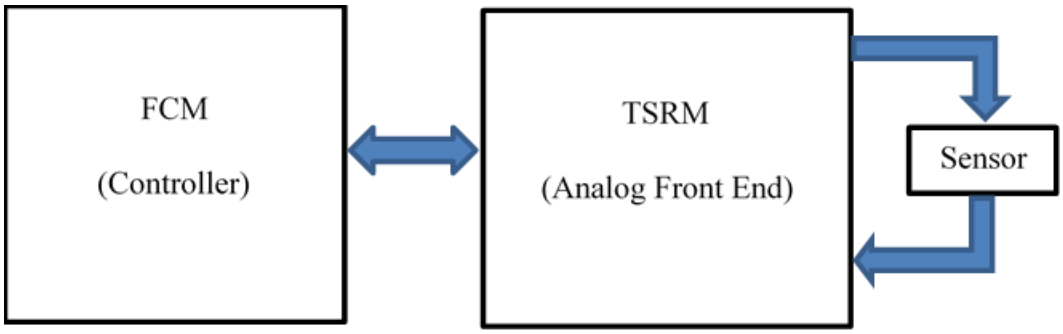

Figure 3.1. Basic functional block diagram of the system.

3.1 Direct digital synthesis.

Direct digital synthesis (DDS) is an algorithm that allows to generate digital form of regular looking periodic signal like a ramp, square or a sinusoid with high flexibility in the control of its frequency, amplitude, and phase. The specific application requirement was to generate sine waves of 10mV RMS amplitude at 100Hz frequency as input for a glucose sensor. The requirement of the signal did not mandate an algorithm that has flexible control on the three parameters but, considering that by allowing flexible control of the frequency and amplitude of the sine wave would allow detection of other biomolecules (non-glucose) DDS was chosen to generate the required sine signal. This choice has made the system versatile to handle many different sensors for detecting different molecules. The other biomolecules that can be detected is limited to those molecules that can be detected using impedance spectroscopy. DDS unit implementation typically consists of five sub-units namely a reference clock, numerically controlled oscillator (NCO), phase to amplitude convertor, digital to analog convertor (DAC) and reconstruction low pass filter (LPF) as shown in figure 3.2.

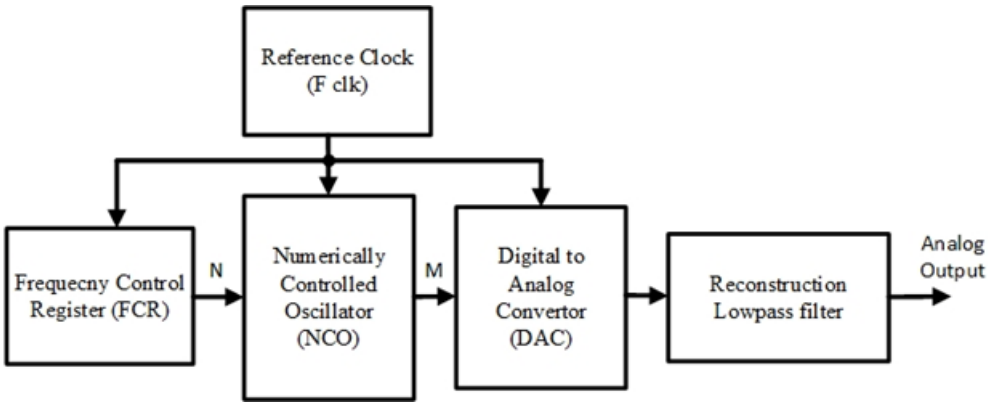

Figure 3.2. Block diagram of Direct Digital Synthesis.

The reference clock is a fixed frequency clock signal which is the timing reference for the DDS unit. The algorithm generates one output sample per cycle of the system reference clock. The frequency of the reference clock has to be several times higher than the maximum required frequency of the sine signal being generated. This would ensure that enough samples are being generated per cycle of the generated signal, thereby allowing successful reconstruction of the generated signal after the DAC.

The numerically controlled oscillator consists of a frequency control register which stores a frequency tuning word (FTW) and an adder accumulator (AAC). The results in the AAC in the NCO forms a periodic ramp shape with respect to time. It generates the ramp signal by continuously adding frequency tuning word FTW at each reference clock. The frequency of the ramp determines the frequency of the generated output signal of the DDS and is therefore dictated by the frequency tuning word. The frequency of the ramp is the same as the frequency of the generated sinusoidal output signal. The equation relating the output frequency the frequency tuning word is

$$f_{out} = \frac{FTW * f_c}{2^n}$$

Where, f_{out} is the output frequency of the generated ramp

FTW is the frequency tuning word

f_c is the frequency of the reference clock and

n is the length of the phase accumulator in bits.

DDS system could also contain a phase word that can adjust the phase of the signal but changing the phase of the sine signal does not serve any purpose in the application. The ramp acts as the phase input to the phase to amplitude converter.

The phase to amplitude converter converts the phase input (ramp signal) to the corresponding amplitude of the required signal. There are several ways of implementing the phase to amplitude converter. It can be implemented as a direct look up table (LUT) where the amplitude of the signal is pre-computed and stored in the look up table in the address locations which corresponds to the phase. This method has the advantage that each clock cycle can generate an amplitude value and there is zero or few clock cycle latency in generating the amplitude value. The size of the look up table becomes prohibitive as the frequency resolution and the amplitude resolution of the signal is large. The size of the required ROM is given by formula below.

$$LUT size(bits) = Amplitude\ resolution\ or\ DAC\ resolution(bits) * 2^{frequency\ resolution(bits)}$$

For a 16 bit DAC and a 32 bit frequency resolution it would require an 8 gigabyte memory. Hence, this method is not used if a high amplitude and frequency resolution is required for the signal being generated. Another method that can be used in the implementation of the phase to amplitude converter is to use CORDIC (COordinate Rotation DIgital Computer) or Volders algorithm. CORIDIC algorithm computes the coordinates of a vector in a x-y plane given the initial x coordinate, y coordinates and the angle it must rotate to reach the new location. It is an algorithm that can be used to compute trigonometric and hyperbolic functions. By restricting the inputs to the algorithm to known initial values, such that initial vector lies in the x-axis with a known magnitude, sine of any given angle can be computed, which in turn serves the purpose of phase to amplitude converter.

3.1.1 CORDIC algorithm

CORDIC Algorithm is an iterative algorithm that can compute coordinate of a vector given an initial vector (x, y) and the angle of rotation (ϕ) to reach the new vector (x', y') as shown in figure 3.3. By setting the proper initial conditions for the algorithm, it can be used to find values of functions like sine, cosine, polar to rectangle, rectangle to polar, linear, and hyperbolic functions.

Instead of finding the $sin(\phi)$ directly in a single step CORDIC algorithm computes $sin(\phi)$ by computing $sin(\beta)$ iteratively, rotating β closer to ϕ in each iteration. The general idea is to fix the initial value of β to $0°$ and rotate it towards θ by adding or subtracting $\frac{45°}{2i}$ where $'i'$ is the iteration count as shown in figure 3.4. With more number of iterations β becomes more closely equal to θ and we get a more accurate approximation of $sin(\phi)$.

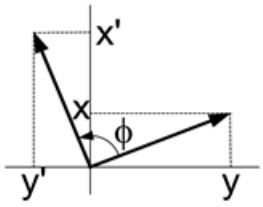

$$\begin{bmatrix} x' \\ y' \end{bmatrix} = \begin{bmatrix} \cos(\phi) & -\sin(\phi) \\ \sin(\phi) & \cos(\phi) \end{bmatrix} \cdot \begin{bmatrix} x \\ y \end{bmatrix}$$

Figure 3.3. New vector co-ordinate (x, y) obtained by rotating a vector (x,y) by ϕ degrees.

In the figure 3.3 the co-ordinate of the new vector can be expressed as

$$x' = x.cos(\phi) \ - \ y.sin(\phi)$$

$$y' = x.sin(\phi) \ + \ y.cos(\phi)$$

which can be written as,

$$x' = cos(\phi)[x \ - \ y.tan(\phi)]$$

$$y' = cos(\phi)[y \ + \ x.tan(\phi)]$$

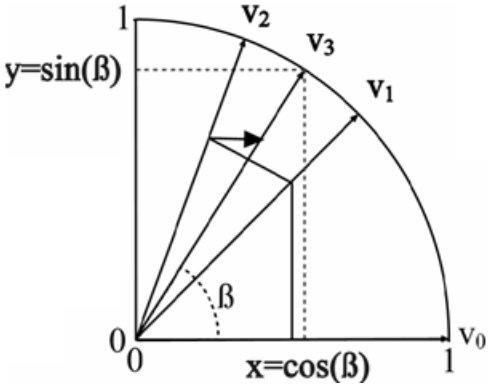

Figure 3.4. Computing vector v_3 starting at vector v_0 and iteratively coming close to v_3

After sufficient number of iterations as β becomes close to θ,

$$x' \approx x_{i+1} \; and \; y' \approx y_{i+1}$$

If we restrict the value of $tan(\beta)$ to $\pm 2^{-i}$, $tan(\beta)$ is the approximation of $tan(\phi)$.
We can re-write the above equation as

$$x_{i+1} = cos(tan^{-1}(\pm 2^{-i}))[x_i \; - \; y_i.d_i.2^{-i}]$$

$$y_{i+1} = cos(tan^{-1}(\pm 2^{-i}))[y_i \; + \; x_i.d_i.2^{-i}]$$

Where, $d_i = \pm 1$ is the direction of rotation. It should be positive if, ϕ is greater than β and negative if, β is greater than ϕ.
Let Z is the difference between the θ and β. We initialize $\beta = 0$ for calculating the sine function and as result Z_0 is initialized to ϕ. We need to have Z close to zero for a good approximation of the sin function. And,

$$z_{i+1} = z_i \; - \; d_i.tan^{-1}(2^{-i})$$

The sign of z_{i+1} gives the sign of d_{i+1}
We can compute x' and y' using simple addition, subtraction and shifting operations if we compensate for the gain of the iterations. $cos(tan^{-1}(\pm 2^{-i}))$ is the gain of each iteration that

is not computed by these simple arithmetic and shift operations. Each rotation introduces a gain factor $\frac{1}{K_i}$ to the vector.

As Cosine is a symmetric function,

$$cos((tan^{-1}(-2^{-1})) = cos(tan^{-1}(+2^{-1})) = K_i = \Pi \frac{1}{\sqrt{1+2^{-2i}}}$$

$As\ n \to \infty, K = \Pi K_i = 0.6037$

So, if we multiply the result by a factor K we will be able to compensate for the gain introduced by the rotation calculated by the simple arithmetic operations.

$$A_n = \frac{1}{K} = \Pi \sqrt[2]{1+2^{-2i}} = 1.647(as\ n \to \infty)$$

Another way is to scale the initial vector by a factor $\frac{1}{A_n} = K$, then the result would be the gain compensated value of the new vector using CORDIC algorithm using simple arithmetic and shift operations.

In summary, calculating $sin(\phi)$ using CORDIC algorithm involves setting the initial vector (x, y) to ($\frac{1}{A}$, 0) and Z_0 to ϕ. Then the values of $x_{i+1},\ y_{i+1},\ z_{i+1}$ (for calculating the direction of rotation) are calculated iteratively until required accuracy is achieved. The $x_{i+1},\ y_{i+1}$ gives $cos(\phi)$, $sin(\phi)$ respectively. The ramp input from the Adder Accumulator is given to Z_0 input of CORDIC to generate the required sine wave of desired frequency.

The advantage of using CORDIC over a direct look-up table is that it requires substantially small memory and its flexibility to generate other functions by just changing the initial conditions. While the direct look up table stores the value of sine function, CORDIC needs to store only the arc tangent values of the angles β and hence need to store very few values compared to direct look up table. The number of arc tangent values stored equals the number of iterations required to calculate $sin(\theta)$ to the required accuracy. The design can be pipelined to achieve higher speeds than a direct look up table at the cost of latency. However, it is more computationally intensive compared to direct look up table and is likely

to consume more power.

The digital to analog converter converts the digital sinusoid word sequences generated by the numerically controlled oscilltor (NCO) to analog voltage levels generating sinusoidal waveform composed of steps changes in voltage levels at each reference clock period. The resolution of the DAC (amplitude and frequency) is usually the bottleneck to the resolution of the DDS system. The final low pass filter removes the high frequency components from the output of the DAC and converts the step changes to a smooth sinusoidal signal. The cut off frequency of the filter should be higher than the maximum frequency of the sinusoid that needs to be generated by the DDS system. A DDS based sinusoid generator was implemented

Figure 3.5. DDS algorithm implemented in FPGA that can produce user specified frequency and amplitude.

in an Artix 7 FPGA and AD5541A DAC module and sinusoids of user inputted frequency and amplitude were generated. This was however not used for the final implementation as there was an existing integrated circuit (AD5933) from Analog Devices that could generate

required sinusoid and calculate the impedance which would result in a more compact design than an FPGA based design. Also, an integrated solution would give better accuracy due to lower losses in the system. The TSRM system was redesigned from an FPGA based system to an off the shelf IC based system and the FCM to a microcontroller based system.

3.2 AD5933 - impedance converter network analyzer

This is the central component in the TSRM module that could measure impedance by generating sinusoids with varying amplitude and frequency and performing a 1024 sample single point DFT on the voltage signal (proportional to the current flowing through the impedance under measurement) generated at the output of the Transimpedance Amplifier (TIA) shown in figure 3.6. It can measure impedances from 1K Ohm to 10MOhm and can be extended to measure impedances from 100 Ohm to 1 KOhm with external circuitry. It can generate output sinusoids of frequency from 1 KHz to 100 KHz sinusoids and can be extended to generate lower frequency sinusoids by scaling the reference clock frequency. It has option to provide an external clock reference or a use it internal 16.7MHz internal clock. It can be configured through an I2C interface and hence the standard interface between the FCM and TRSM was selected to be an I2C interface. The rest of the system was designed around the AD5933. The remaining programmable components in the system were chosen to be I2C based devices as a result. The AD5933 generates a sinusoid using the DDS algorithm same as in the Artix 7 based implementation of a sine wave generator. It can be configured to use its internal clock or an external clock as the reference clock to the chip. This reference is used for DDS core as well as sampling clock in the 12-bit ADC in the system. An external clock is required in generating a 100Hz sinusoid because 1024 samples of the internal clock frequency will not include even a complete cycle of a 100Hz signal. The maximum external clock frequency that can be used to generate a 100Hz (0.01 sec period) signal is to use a 100KHz external clock. One KHz is the minimum AD5933 datasheet recommended frequency of the

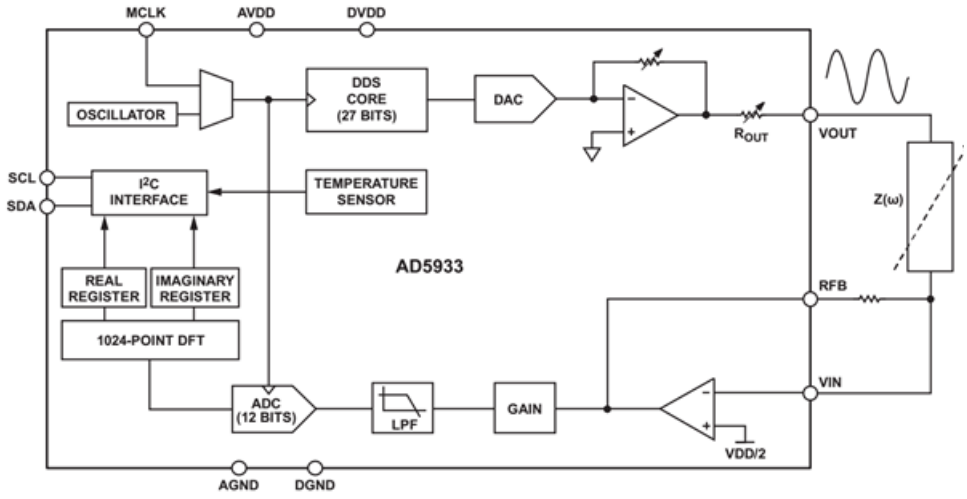

Figure 3.6. Functional Block diagram of AD5933 [7].

sinusoid that is to be generated using the internal clock source. This suggest for a need for a programmable reference clock source to scale per the requirements of output sinusoid frequency. This source need to be configured by the FCM and should communicate through the same standard I2C interface. The I2C based programmable clock source from linear technologies LTC6904 was used to serve this function. It can be configured to generate clock signal from 1KHz to 68MHz as per the requirement of the system.

The DDS core can be configured using I2C to generate a specific frequency or do a frequency sweep from a programmable start frequency to a stop frequency with required step size. The amplitude can also be programmed to select from four different choices. 2V peak to peak biased at 1.48V, 1V peak to peak biased at 0.76V, 400mV peak to peak biased at 0.31V and 200mV peak to peak biased at 0.173V are the four choices given by the AD5933. The application required 10mV RMS or 28mV peak to peak sinusoid signal to be generate so 200mV amplitude can be selected and external circuitry can be used to attenuate the signal and bias it at the required voltage. The output of the DDS block in figure 3.6 goes to DAC followed by a programmable gain amplifier with gain of 1 or 5. The generated sinusoid is applied to the impedance (sensor) that is external to the chip and it forms the input to the

trans impedance amplifier in AD5933. The voltage output of the trans impedance amplifier which is proportional to the current flowing through the impedance(sensor) is sampled by a 12-bit ADC at the reference clock. 1024 samples from this ADC along with samples from DDS core are used by a single point DFT core to generate a complex number that is proportional to the current flowing through the sensor or admittance of the sensor. It gives two 16 bit real and imaginary register values as the output of the DFT and can be read by the FCM through the I2C interface. With proper calibration, these register values can be used to calculate the impedance of the sensor. The variation of the impedance of the sensor from baseline after the sweat sample is added can be used to calculate the glucose concentration in sweat [4].

3.3 Analog signal conditioning chain

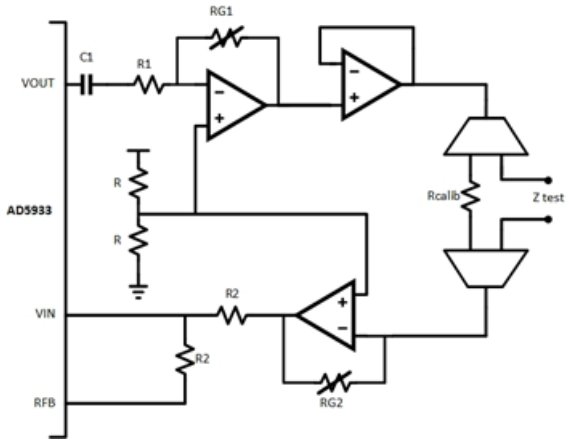

Figure 3.7. The analog front end designed to work with the AD5933.

The voltage signals that can be generated by the AD5933 does not match in amplitude and bias requirements of the glucose sensor. The sensor requires a 10mV RMS sinusoid to be applied across it two terminals with a zero DC bias. There is only limited choice of signal amplitude and DC bias that the AD5933 can be configured to generate. The available choices in signal amplitude and associated DC bias that the ad5933 can generate are given

Table 3.1. The ideal values four-different sinusoid voltage signal amplitude that can be generated by AD5633 and its corresponding DC bias level for 3.3 V supply.

Range	**Signal Amplitude**	**Associcated DC bias**
Range 1	1.98 V_{pk}	1.48V
Range 2	0.97V_{pk}	0.76V
Range 3	383mV_{pk}	0.31V
Range 4	198mV_{pk}	0.173V

in table 3.1 for a 3.3V supply. The supply voltage can range from 2.7V to 5.5V and the signal amplitudes and DC bias levels scale linearly with supply voltage.

There is a need to design an analog signal conditioning chain from the AD5933 signal output pin (vout) to the sensor (impedance to be measured) and from the senor back to the input (vin) and feedback(rfb) pins of the AD5933. The AD5933 works on a single supply and hence the output signal cannot be biased at ground as the signal would be clipped off in the negative side so a virtual ground should be used to bias both ends of the sensor. The vin pin shown in figure 3.3 is internally biased at VDD/2 and hence the virtual ground point is fixed at VDD/2 (1.65V). This also ensures that there is maximum head and leg room for the output signal swing. A 10mV RMS (28mV p-p) signal is to be generated and applied to the sensor. The signal is smaller than the smallest signal amplitude generated by the AD5933 as seen from table 3.1. The DC bias of 0.173 V must be removed using a high pass filter. The 198mV p-p signal must be attenuated to a 28mV p-p and the signal must be rebased at 1.65V before applying the sinusoidal signal to the sensor. This can be achieved using an inverting amplifier configuration of an op-amp. This conditioned signal can then be applied to one the sensor terminals. The signal has 180-degree phase shift and can be removed by adding another inverting amplifier configuration of an op-amp connected to the other terminal of the sensor. This op-amp must be also biased at VDD/2 to ensure that the difference in DC bias between the terminals of the senor is zero. The output of this stage can then be fed to the input pin (vin) after configuring the gain of the internal op-amp to

be gain of the internal input op-amp of AD5933 to unity. This done by the two equal valued resistors connected to the vin and rfb pins of AD5933.

3.4 Configuring the AD5933

The AD5933 register map is shown in table 3.2. It consists of registers that can be configured by an I2C master device. It allows you to do a frequency sweep and read the results at each frequency to find out the impedance response of the device. The frequency range and step size of the sweep can be specified using the start frequency, frequency increment and number of increments register in the register map. By configuring the start frequency to 100Hz and step size to zero, a single frequency measurement can be done. Multiple readings in the same frequency can be done by setting the Number of Increments register with the required measurement count.

The number of settling cycles indicates the time to wait before the ADC starts sampling the output in terms of number of output cycles. This allows to start measurement after a certain wait time after applying the inputs which if needed can be used to wait until the system reaches a steady state. The status register indicates if a single frequency measurement is completed and whether the entire frequency sweep is completed. Once a measurement is complete, the results in real register and imaginary register is read out and if required, a new measurement can be initiated by sending increment frequency or repeat measurement command to the control register.

The control register does many configuration as well as control functions in the operation of AD5933. The values in control register is shown in table 3.3. It is used to configure to use external or internal clock source, select the voltage output range from the four available options, select the gain of the programmable gain amplifier to x1 or x5. It is used to put the device in normal, power down or standby mode. It can be used to control the measurement process by giving commands to initialize the output with start frequency, start a sweep and

Table 3.2. The register map of the AD5933 used to configure it for impedance measurement [7].

Register	**Name**	**Bits**	**Read/Write**	**Function**
0x80, 0x81	Control	16	R/W	Control Register
0x82, 0x83, 0x84	Start Frequency	24	R/W	Frequency to start sweep
0x85, 0x86, 0x87	Frequency Increment	24	R/W	Step size of sweep
0x88, 0x89	Number of Increments	16	R/W	Increments in sweep
0x8A, 0x8B	Number of Settling Cycles	16	R/W	Wait time in output cycles
0x8F	Status	8	R	Status of operations
0x92, 0x93	Temperature	16	R	Internal IC temperature
0x94, 0x95	Real Data	16	R	Real part of result
0x96, 0x97	Imaginary Data	16	R	Imaginary part of result

ADC measurement, increment frequency, repeat frequency, measure temperature or reset the sweep. The status register has three MSB bits that indicate if the device register has valid temperature value, real/imaginary values and weather frequency sweep is complete. The remaining 5 LSB bits are reserved.

The control register does many configuration as well as control functions in the operation of AD5933. The values in control register is shown in table 3.3. It is used to configure to use external or internal clock source, select the voltage output range from the four available options, select the gain of the programmable gain amplifier to 1 or 5. It is used to put the device in normal, power down or standby mode. It can be used to control the measurement process by giving commands to initialize the output with start frequency, start a sweep and ADC measurement, increment frequency, repeat frequency, measure temperature or reset the sweep. The status register has three MSB bits that indicate if the device register has valid temperature value, real/imaginary values and weather frequency sweep is complete. The remaining 5 LSB bits are reserved.

3.5 The FCM module

The FCM module was chosen to be an Arduino prototyping platform because it has several variants with a standard pin interface to connect with its shields. Shields are boards that

can be connected to an Arduino that gives additional hardware functionality to Arduino. If the TSRM was designed with the standard interface of an Arduino shield, then we can choose the appropriate variant of the board to function as FCM with just enough memory and other resources to run the program. This standard interface in different boards for connecting to its shields allow us to swap the FCM module. The same TSRM was used with two variants of this platform namely Arduino Mega 2560 and Arduino Uno without any hardware modifications to the TSRM or FCM. The other important factor to use this as the FCM module is because it allows quick prototyping as it has well established online community and abundance of code examples. It also has the required I2C interface that can be used as the standard interface between the controller and other configurable parts in the TSRM.

There are several sub-functions that the FCM module implements to calculate the glucose concentration in sweat as shown in figure 3.8. The functions include setting the external clock frequency, setting the AD5933 clock to external clock source, setting gain of the PGA, selecting the voltage range of the sinusoidal output from the four choices, reading device temperature, setting the settling time in terms of number of output sinusoid cycles to wait before the ADC starts to sample, setting the start frequency, step size and number of frequency increments in the required frequency sweep. connecting the output to a known impedance and start the frequency sweep, using the know value of the impedance and the measured values to calculate the calibration gain factor of the system and system phase, switch the output to the sensor and measure the impedance of the baseline sensor without any glucose in it, measure the impedance of the sensor once the glucose is added to the sensor, calculate the impedance difference from baseline and use the percentage change in impedance to calculate the concentration of glucose present in sweat sample.

Table 3.3. AD5933 control register map [7].

Bits	Value	Description
D15:D12	0000	No Operation
	0001	Initialize with start frequency
	0010	Start frequency sweep
	0011	Increment frequency
	0100	Repeat frequency
	1000	No operation
	1001	Measure temperature
	1010	Power down mode
	1011	Standby mode
D10:D9	00	2.0 V p-p Output voltage range
	01	200mV p-p Output voltage range
	10	400mV p-p Output voltage range
	11	1 V p-p Output voltage range
D11	No Operation	
D8	0	PGA gain x5
	1	PGA gain x1
D7	Reserved; Set to 0	
D6	Reserved; Set to 0	
D5	Reserved; Set to 0	
D4	Reset	
D3	1	External System Clock
	0	Internal System Clock
D2	Reserved; Set to 0	
D1	Reserved; Set to 0	
D0	Reserved; Set to 0	

3.6 AD5933 calibration and impedance measurement

The AD5933 performs single DFT on the 1024 samples from ADC and gives a complex number, call it D; which is stored a 16-bit real word (real(D)) and a 16-bit imaginary word (imaginary(D)). The complex word D is not the complex impedance. The DFT algorithm is given by

$$X(f) = \sum_{n=0}^{1023} (x(n)(cos(n) - jsin(n))) \tag{3.1}$$

Where, X(f) is the power in the signal at frequency point $f, x(n)$ is the ADC output and $cos(n) and sin(n)$ are the sampled test vector from the DDS core [7]. This DFT calculates the energy at a given frequency. This magnitude of the result (D) is proportional to current flowing through the sensor or the admittance sensor and is given by

$$Magnitude\ of\ D\ = \mid D \mid = \sqrt{real(D)^2 + imaginary(D)^2}$$

The phase difference between the voltage input and the current is given by

$$Phase(rads) = \phi = tan^{-1}\left(\frac{Imaginary(D)}{Real(D}\right)$$

This however is does not correspond to the actual value of admittance or inverse of impedance of the sensor. A resistor of known value is connected between the output and input terminals of the AD5933 and the value of Magnitude and System Phase (ϕ_{system}) are calculated. The gain factor that relates the impedance to the measured magnitude is calculated and this multiplication factor is used to calculate actual values of impedance from the measured magnitude when an unknown impedance is connected between the measurement terminals. The gain factor can be calculated as given below

$$\mid D_{calibration\ resistor} \mid \propto Admittance\ of\ CalibrationResistor$$

$$\mid D_{calibration\ resistor} \mid \propto \frac{1}{Calibration\ Resistance}$$

$$\mid D_{calibration\ resistor} \mid = Gainfactor\ * \left(\frac{1}{Calibration\ Resistance}\right)$$

$$Gain\ factor = \frac{1}{Impedance * \mid D_{calibration\ resistor} \mid}$$

This is the gain factor of the system. The phase measure during this calibration phase is the phase difference caused by the system (ϕ_{system}) as a connected resistance does not cause any phase change. This value is noted down as system phase. Once the gain factor is computed an unknown impedance can be measured by

$$Unknown\ Impedance(Z_{unknown}) = \frac{1}{Gain\ Factor * \mid D_{Unknown\ Impedance} \mid}$$

The phase measured with unknown impedance is the sum of system phase measured during calibration phase and the phase change caused by the impedance. The phase of the unknown impedance can be calculated as

$$\textit{Phase of Impedance } (\phi_Z) = \textit{Phase measured with unknown impedance}(\phi_{unknown}) \textit{ - Phase measured with calibration resistor } (\phi_{system})$$

Once the magnitude and phase of the impedance can be determined concentration of glucose can be measured using the curve fitting equation detailed in or using the look up table detailed in chapter 2 from [4].

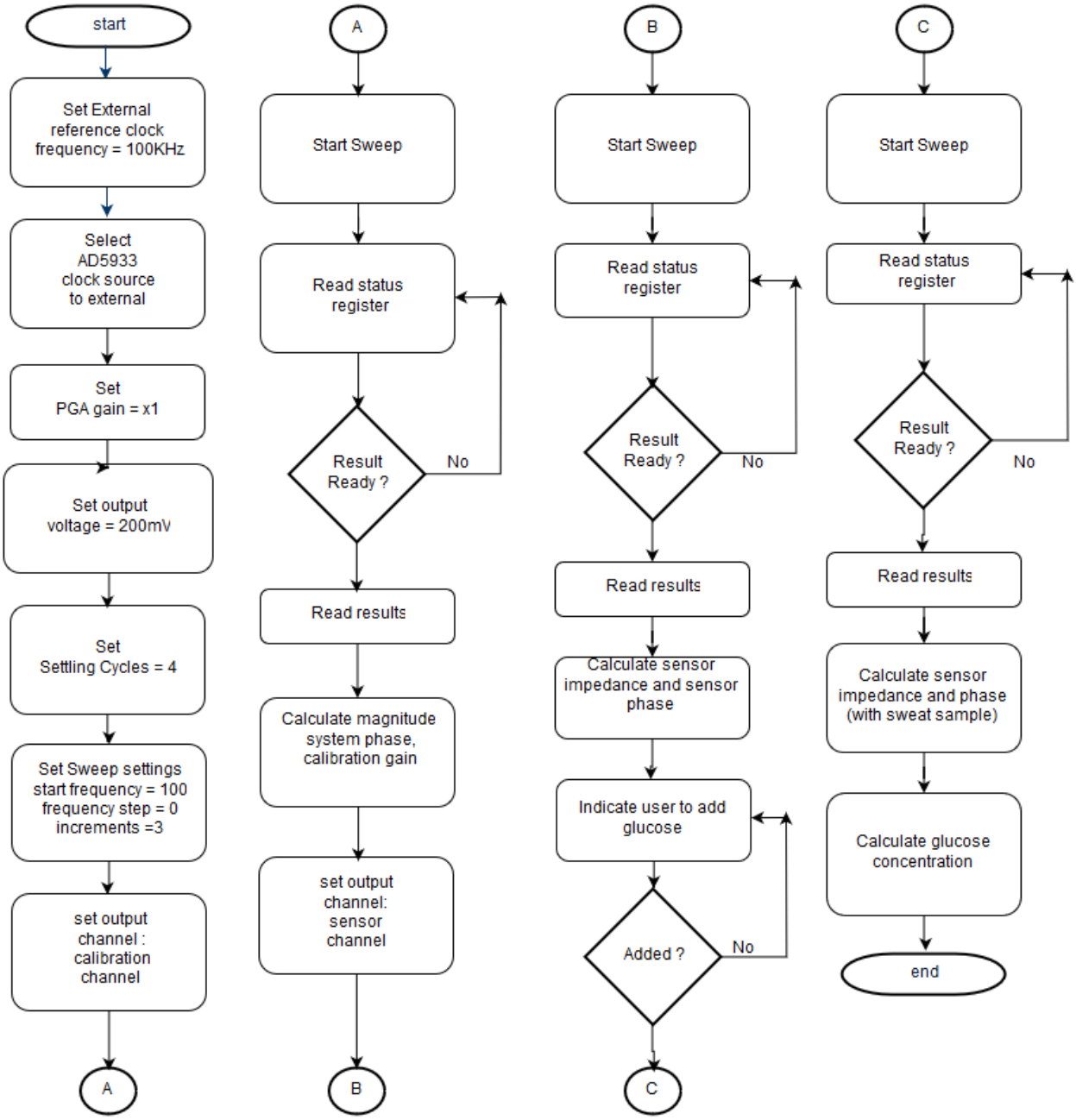

Figure 3.8. Flowchart of the sweat glucose measurement program.

CHAPTER 4

SYSTEM DESIGN IN PCB

System design in PCB is the final design step in most electrical systems. It is done once the design is tested using prototype circuits made in breadboard or using evaluation boards. The printed circuit board (PCB) for the system was designed in the free Eagle CAD Educational Software version 7.7. It supports 99 schematic sheets and 6 layers of signals with maximum routing area of 160mm x 100mm. However, only two signal layers and two schematic pages were used in the TSRM board that was designed and it resulted in 80mm x 50mm board (slightly smaller than a credit card). This board is called the CIMD (Configurable Impedance measurement device). The dimension of this board was fixed to match the dimensions of an Arduino shield.

The Arduino prototyping platform is the FCM module for the designed system. There is a large variety of Arduino boards available commercially that are code compactible and have very well established online documentation. In addition to that, all Arduino boards have a standard interface to its shields and hence it gives the choice of the selecting any Arduino variant as the FCM module depending on the complexity of the functions that needs to be handled by the module. The developed firmware was tested in the Arduino UNO Arduino MEGA boards without making any modifications. It could also be tested in Arduino BT (Bluetooth variant) and make the device wirelessly communicate to a smartphone application using Bluetooth without much modifications. Thus, by using Arduino as the FCM, the task of designing the PCB for FCM was eliminated, while maintaining some flexibility in cost, power, and board size and capabilities.

4.1 PCB design

The steps involved in PCB design include component selection and creating a schematic, placement, routing, creating the bill of materials, design rule check and ordering the PCB

and the components. The final step involves soldering the components together and testing the completed board for its functionality and identifying the limits of performance of the board.

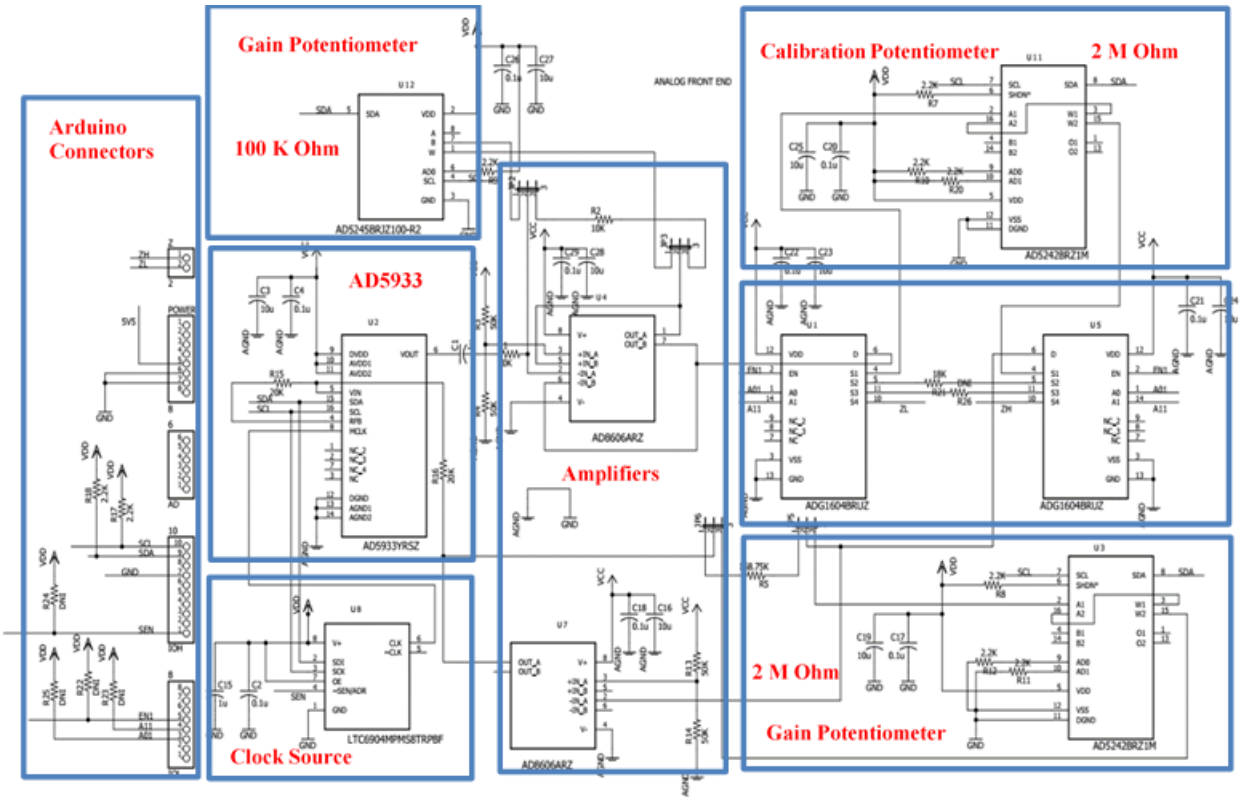

Figure 4.1. Schematic of the Analog Front End (AFE)

4.1.1 Component selection and schematic design

One of the most important parts of schematic design is identifying the components and package for the parts in the system design. The conservative and safe approach would be to use the components used in the prototype system or the evaluation boards. Once this is implemented and tested you could replace the component parts that give you some advantage in terms of cost, power, or area in the next revision of the board along with any required bug fixes. There is a tradeoff between cost, size, power, availability in choosing the right part for

your application. The smallest package that you can use is also limited by the equipment required to solder the part together in the board. A plan of where the parts will be placed in the board will also help in selecting the correct parts. The component ICs in the configurable

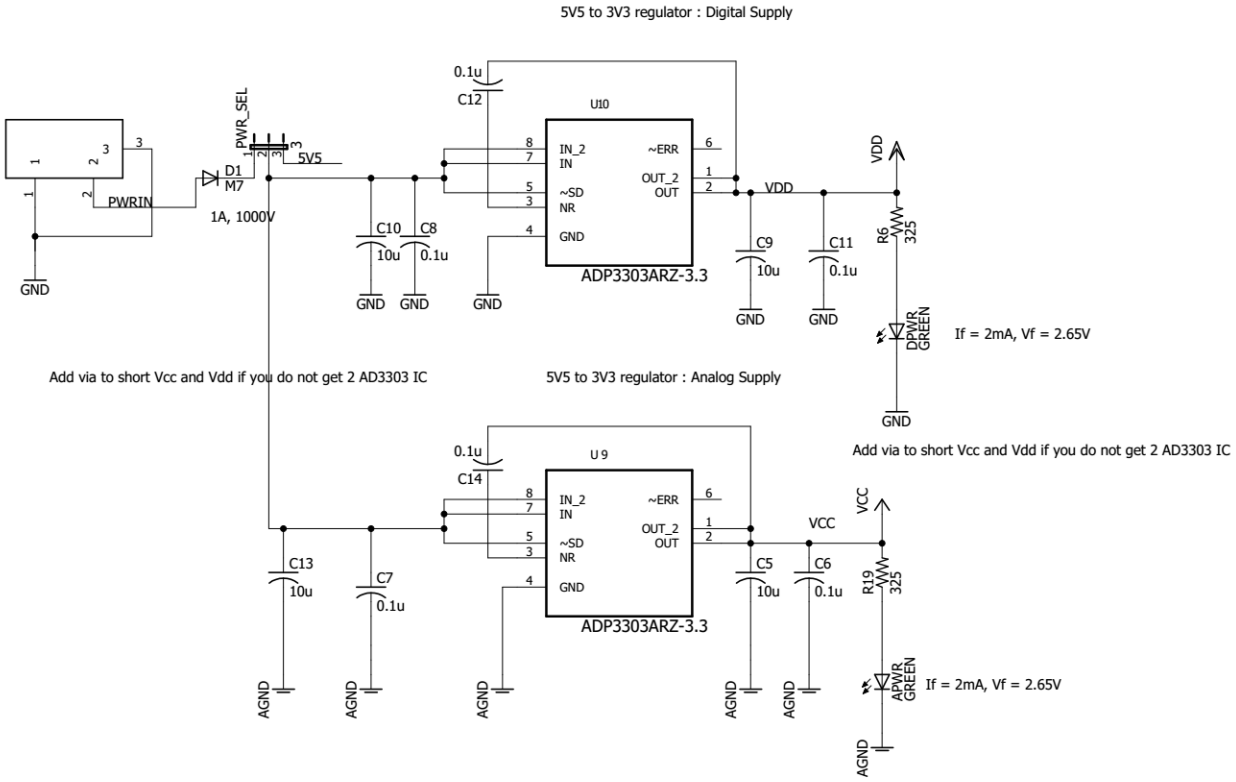

Figure 4.2. Schematic of the Power supply system showing separate power supplies rails for analog and digital sections of the design

impedance measurement device (CIMD) was either classified as either digital or analog and there are separate power lanes for each of these partitions. The mixed signal IC AD5933 was also considered as an analog IC. The grounds traces of the analog and digital and part of the system as connected only at one single star point to reduce the noise from the digital circuit and switching to affect the analog part of the design. Once the components are finalized the schematic can be competed as shown in figure 4.1 and figure 4.2.

4.1.2 Components of the TSRM system

The functionality and capabilities of the components used in the TSRM system are briefly explained in the following section. These include integrated circuit namely, AD5933, ADP3303, AD8606, LTC6904, ADG1604, AD5242BRZ1M and AD5245BRJZ100. Samples of these ICs were obtained from Analog Devices and Linear Technologies to build two boards.

AD5933 (1MSPS, 12-Bit impedance converter network analyzer)

The AD5933 is a high precision impedance measurement system that has an inbuilt DDS based frequency generator, 12-bit ADC to sample response signal from the impedance, and a DSP engine to perform a 1024 sample single point single DFT to generate a complex word that is the measure of the power of the response signal from the impedance at the frequency generated by the DDS. With calibration using a resistance of known value that is in the range of the unknown impedance to be measured, unknown impedance can be measured using the AD5933.

ADP3303 (High accuracy 200mA low dropout linear regulator)

This is the linear regulator that gives constant 3.3V output and 200mA current to power the TSRM. This is low noise linear regulator that has dropout voltage of 180mV at 200mA. Two separate ADP3303 where used to power the digital and the mixed signal components in the system. The input supply to this can be selected from either an external power adaptor of from the Arduino board.

AD8606 (precision, low noise, RRIO, CMOS Op Amp)

AD8606 is a precision dual op-amp with low maximum input bias current of 1pA. It has bandwidth of 10MHz and has a high open loop gain of 1000V/mV. It is a single supply op amp that can operate from 2.7V to 5.5V. Two AD8606 were configured as two amplifiers and

a unity gain buffer. These chips are used in the analog front end to AD5933 attenuate the signal to make it in the desired 10mv RMS from a 200mV p-p while support drawing more current than the AD5933 can support by itself. Another function of the analog front end is to bias both terminals of the measured impedance to fixed 1.65V (VDD/2) and remove the 0.176V bias. A single quad op-amp AD8608 can be used to replace the two AD8606 to reduce board area.

LTC6904 (1 kHz -68 MHz serial port programmable oscillator)

This is the external reference clock that can generate the required reference clock frequency for the AD5933. It is a single supply chip that can operate from 2.7V and 5.5V. It can generate single or differential clock signal of frequency range 1 KHz to 68 MHz and can be programmed to using an I2C master device. It is used to make sure that as the DDS output frequency is scaled down the ADC is capturing at least a complete cycle in 1024 samples of the output signal to compute the DFT. The ADC also uses the reference clock frequency used by the DDS to sample the response signal form the impedance. This implies that there is a penalty in speed of ADC sampling and DFT processing that must be incurred to get accurate results when the DDS is configured to generate low frequency output sinusoid.

ADG1604 (4:1 analog multiplexer)

AD1604 is a 4:1 analog multiplexer that can has very small on resistance of 1Ohm and operated bidirectional. It can operate single or dual supply from +/- 5V or +12V. It is used to switch between the calibration impedance or unknown impedance to apply the signal generated from AD5933. This allows for the TSRM to be calibrated without any manual intervention. Moreover, it also gives the option to add multiple calibration resistances. The calibration impedance used must be close to the unknown impedance in magnitude to get good accuracy in impedance measurement. Hence, having multiple calibration impedance channel would increase the range of impedances that can be measured accurately.

AD5242BRZ1M (Dual-channel, I2C compatible, 256 position, digital potentiometer)

It is a 1 M Ohm programmable digital potentiostat that can be configured using I2C to be a resistance of any value up to 1 M Ohm in steps of 4K Ohm. It is used to configure the gain of the AD8606 such as a manner that the output of the amplifier does not saturate or become too low to be submerged in noise with a large range of unknown impedance. It is also used as calibration impedance that can be used to when unknown impedance is to be measured.

AD5245BRJZ100 (256 position I2C compactible digital potentiometer)

It is a 100K Ohm programmable digital potentiostat that can be configured using I2C to be a resistance of any value up to 100K Ohm in steps of 400 Ohm. It is used to attenuate the AD5933 output signal to the 10mV RMS amplitude that sensor requires. It can also be used to amplify the output because it is used as the gain setting feedback resistor in the AD8606 amplifier. The gain can range from 0.006X (attenuation) to 1.5X (amplification). This flexible gain setting along with the choice of four amplitude ranges of AD5933 allows us to generate any sinusoid from 2mV to 3V peak to peak for a power supply voltage of 3.3V. This range scales linearly with the used power supply voltage from 2.7 V to 5.5V.

4.1.3 Placement and layout

The schematic when exported in to a layout view of the eagle, gives a rat-nest view of the design. It consists of a board area defined by a rectangular boundary and area outside it as shown in figure 4.3. Initially, all component ICs in its actual physical representation is placed outside the board area. The equivalent connections in the schematic are represented as air-wires that forms a mesh of connections. The first task is to manually place the components inside the board area and finalize the placement of all components. The mesh of air wires

must be untangled as much as possible to make routing feasible to complete less board area and layers. Once the placement of the components is completed, each air wires can be routed to a physical track with required width. The width of the wires is specified in mils (1/thousand of an inch). The required track width can be calculated based on the current

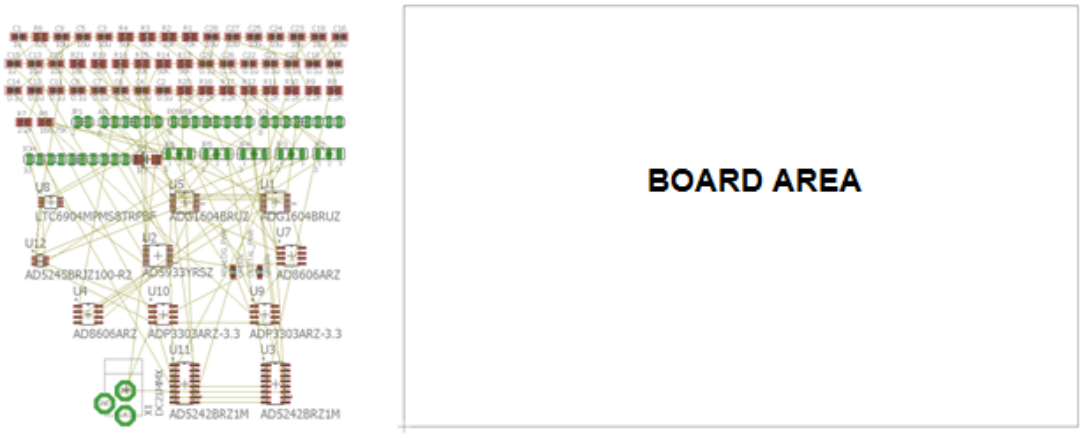

Figure 4.3. Initial board layout view showing components and air wires outside the board area

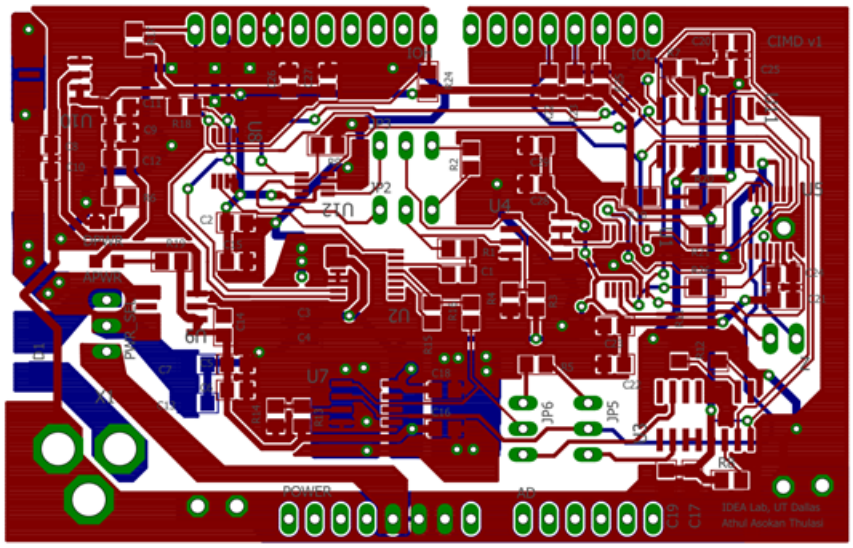

Figure 4.4. Completed Layout of the system

that it needs to handle and the thickness of the copper cladding used for tracks. The track

width can also depend on the temperature of operation of the board and the length of the track. There are many online trace width calculators that can be used to calculate the trace width. Wider tracks offer lower resistance for the same trace length than a smaller width track. Higher the thickness copper can give lower resistance but is generally more expensive to have PCB with thicker tracks. The ground signal in the board can be spread across the board area rather than being a wire. The ground plane ground plane can be seen in the 3D model shown in figure 4.5. The completed layout of the CIMD can be seen in figure 4.4. Once the layout is completed the design rule check (DRC) and electrical rule check (ERC) is

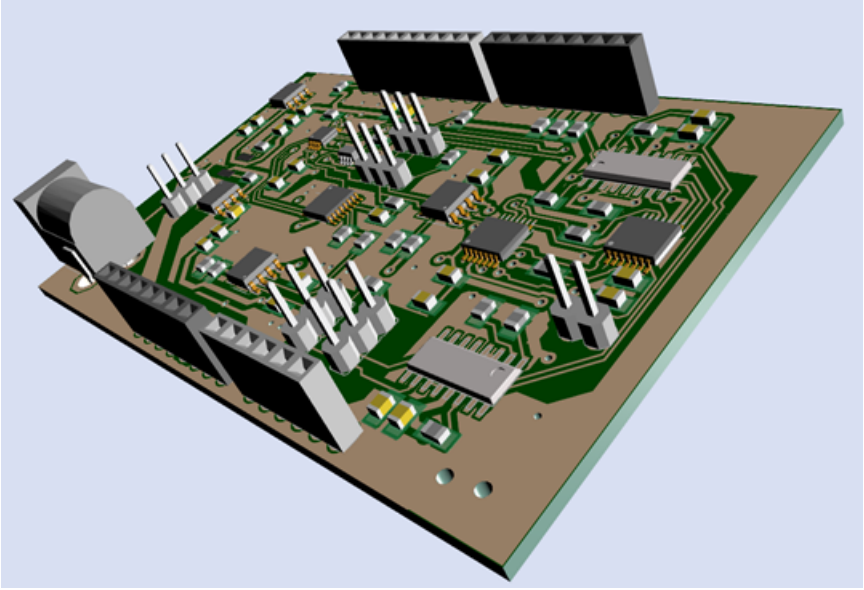

Figure 4.5. Three-dimensional model of the PCB (top side)

done to make sure the schematic and layout match and the minimum spacing and size rules are followed in the design. The errors in the design are fixed before the gerber files for the layout and drill files for via are created using CAM processor. The design must be verified by for manufacturability using the design for manufacturing (DFM) check offered by the PCB manufacturer. Once the errors in DFM check are cleared we can view the design using gerber views to ensure that the board looks as your expectations. 3D model of the PCB can also be generated to make sure the board design meets your expectations in size and final form

factor. The 3D models for the TSRM board is shown in figure 4.5 and figure 4.6. The board can then be sent for manufacturing and the components in the bill of materials ordered or sampled. The completed board that came from the PCB manufacturer (Advanced Circuits) is shown in figure 4.7. The board once tested for connectivity and visually inspected can be used to mount the components and solder them to complete the PCB as shown in figure 4.8. The passive components can be measured using a digital multimeter before soldering it in

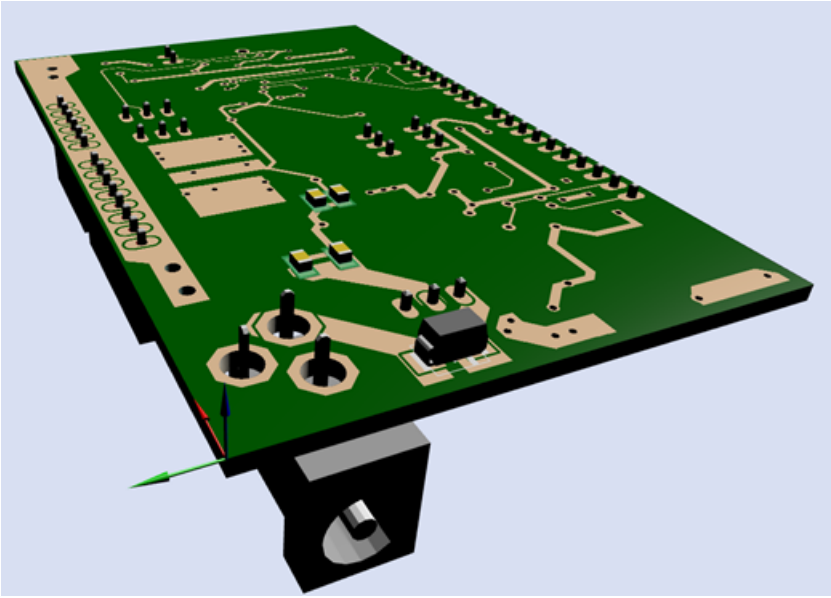

Figure 4.6. Three-dimensional model of the PCB (bottom side)

the board, however most of the integrated circuits can be tested only once they are mounted in the board. The power supply regulator chips can be mounted first and tested to make sure the supply is giving expected line regulation before the rest of the ICs are mounted This would prevent damage that could arise from faulty power supply chips or power supply traces.

4.2 Complete system

The complete impedance measurement device includes the Arduino board, the custom designed CIMD (configurable impedance measurement device) and a Zigbee based wireless

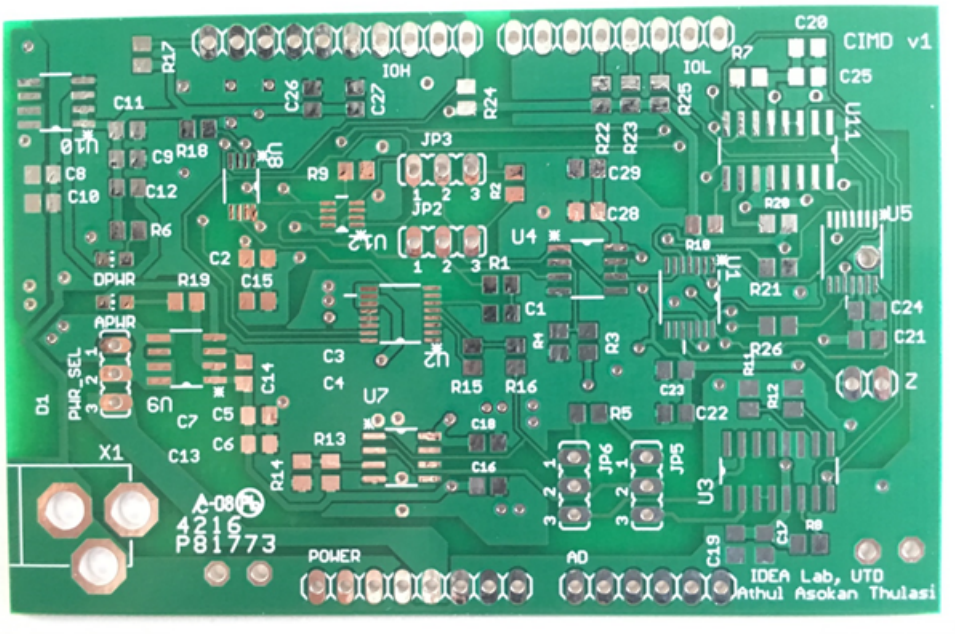

Figure 4.7. The manufactured PCB board from Advanced Circuits (top side)

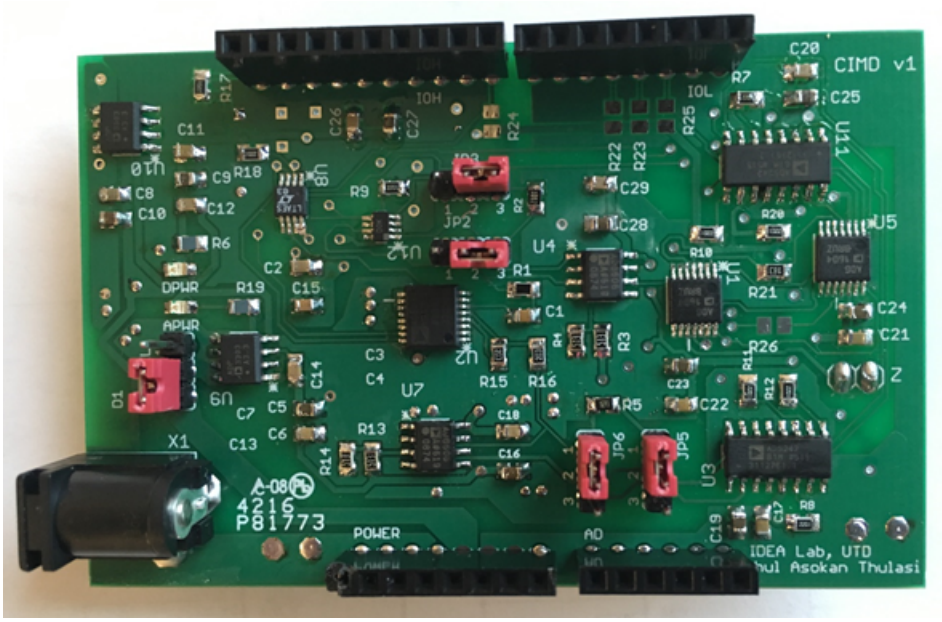

Figure 4.8. CIMD populated with the all components.

module powered by battery on the measurement side and a laptop with a Zigbee module connected to USB port. The XCTU Zigbee configuration software installed in the laptop re-

ceives the data send by the transmitter side and send commands to the transmitter side. The XCTU Zigbee configuration software is used to configure the Zigbee modules to communicate to each other by setting them in same channel, network and baud rate.

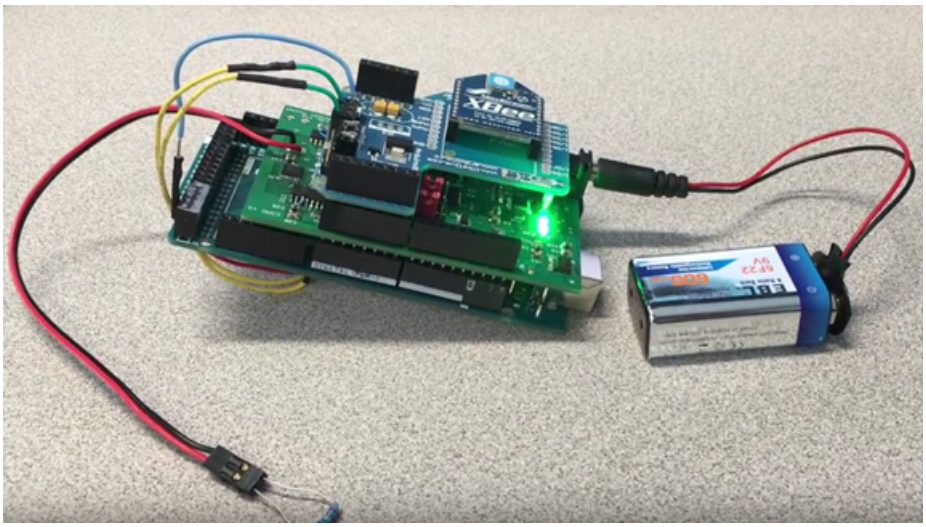

Figure 4.9. Complete transmitter side prototype with Arduino, CIMD and Zigbee.

4.3 Characterizing the system

The board had to be tested for proper functionality before it can be characterized to find the limits of its operation. There were several minor hardware bugs in the board layout which were fixed in layout as well as patched in the existing prototype boards by removing some traces and adding traces using wires. Once these issues were fixed, the board was tested to find it limits of operation. The hardware bugs in the board included miswiring of positive and negative terminals of the gain setting op-amp AD8086. The I2C address of in AD5242 and AD5245 used in the system turned out to be the same (0x2C) due to improper wiring of the address selection pins. This was fixed by chaining the address of AD5245 to 0x2D by rewiring the address selection pin to VDD instead of ground. There was also an open circuit in the internal connection of AD5242 which could be fixed by a slight rewiring in the pin connections in the IC.

4.3.1 Range of output frequency

The CIMD clock source LTC6904 can generate the reference clock with frequency range from 1KHz to 68MHz hence a DDS system should be able to generate an ideal maximum frequency of 34MHz (fmax/2 per Nyquist criteria). However, the DAC in the DDS system is not perfect and it usually attenuates the output as the output frequency get closer to the reference frequency. The aliased images of the output frequency will have higher energy as the output frequency gets closer to the reference clock frequency. The maximum frequency that can be generated depends on the DAC as well as the low pass filter specifications. The AD5933 data sheet specifies the maximum frequency of output sinusoid that can be generated as 100KHz with the internal clock frequency of 16MHz. The smallest recommended frequency that can be generated is 1 KHz using the internal clock and 0.1KHz with a reduced clock frequency of 500KHz. The designed system can operate in any frequency from 10Hz to 100KHz with very good frequency resolution. It can also generate frequencies out of this range, from 1.3Hz to 2MHz as shown in figure 4.9.

4.3.2 Range of output amplitude

The amplitude of sinusoid that can be generated by AD5933 is limited to four different values as shown in table 3.3. However, that external analog front end has gain setting that enable us to generate any voltage amplitude required from 4 mV p-p to 3Vp-p for a 3.3V supply as shown in figure 4.9. The range linearly scales with the power supply voltage from 2.7V to 5.5V. Any of the four ranges in AD5933 can be chosen and the gain setting resistor can be set to attenuate of amplify the signal. The system also can support measuring the entire range of impedance supported by the AD5933 i.e., from 1K Ohm to 10MOhm.

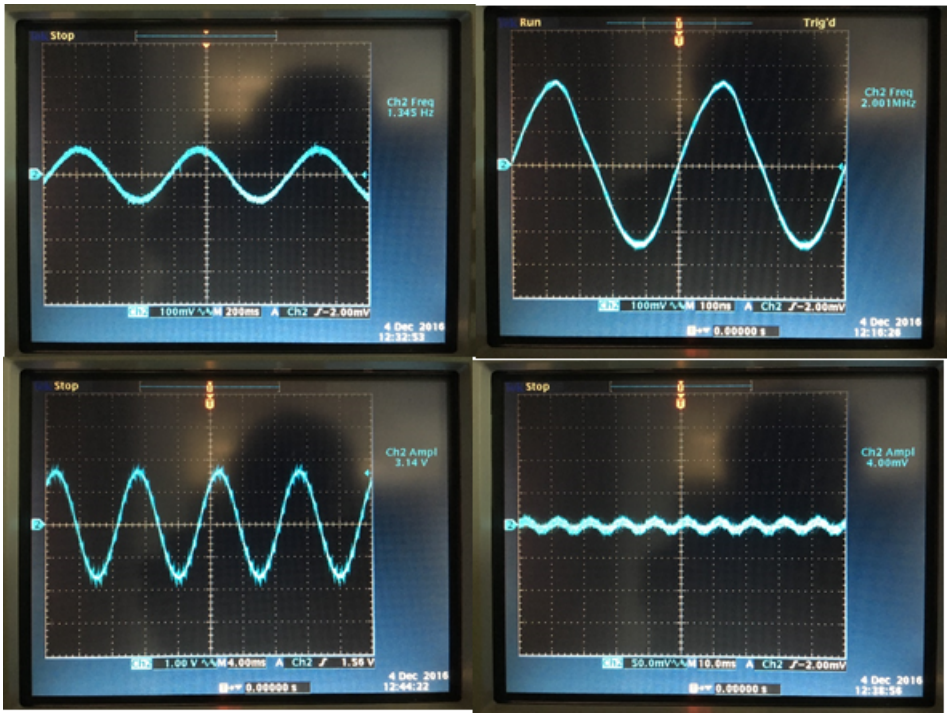

Figure 4.10. Oscilloscope outputs showing the frequency and amplitude limits of CIMD.

CHAPTER 5

EXPIRIMENTS AND SYSTEM TESTING

This chapter deals with all the board level test and measurement that were used to test the functionality of the board. It explains the test procedure and test results and inferences from the test. These tests results gave a better insight in to the working of the system and helped to optimize the performance of the system.

5.1 Device calibration resistance measurement test

This is a basic sanity check for the device functionality. The CIMD needs to be calibrated using a standard resistance of known value before it can measure an unknown impedance. Once the system is calibrated the device is used measure the same calibration resistance. A 18K Ohm 0.1% tolerance resistor was used to calibrate the device for measuring the glucose sensor impedance from the range of 8K Ohm to 20K Ohm. The value of the calibration impedance was measured to be 18.06K Ohm using a Digital Multimeter. The CIMD FCM firmware used 18K Ohm as the value of calibration resistance for calculations and calibrated the device. Forty measurements of the calibration impedance followed the calibration procedure. The mean of the measurements came out to be 17926.51 Ohm (expected 18K Ohm) with a standard deviation of 26.31 Ohms (0.15%). The plot showing absolute variation of the measured resistance from the mean of the measured resistance if shown in figure 5.1 The error in measurements was calculated taking 18K Ohm is the actual value of the calibration resistance. The mean of the error was 73.26 Ohm (0.4%) and the standard deviation of the error was 26.31 Ohms (0.15%). The actual value of the calibration impedance is 18.06K Ohm per the digital multimeter. The CIMD FCM module firmware was adjusted to have the calibration resistance to 18.06 K Ohm and the experiment was repeated. The mean of the measurements came out to be 18040.57 Ohm (expected value of 18.06K Ohm). With

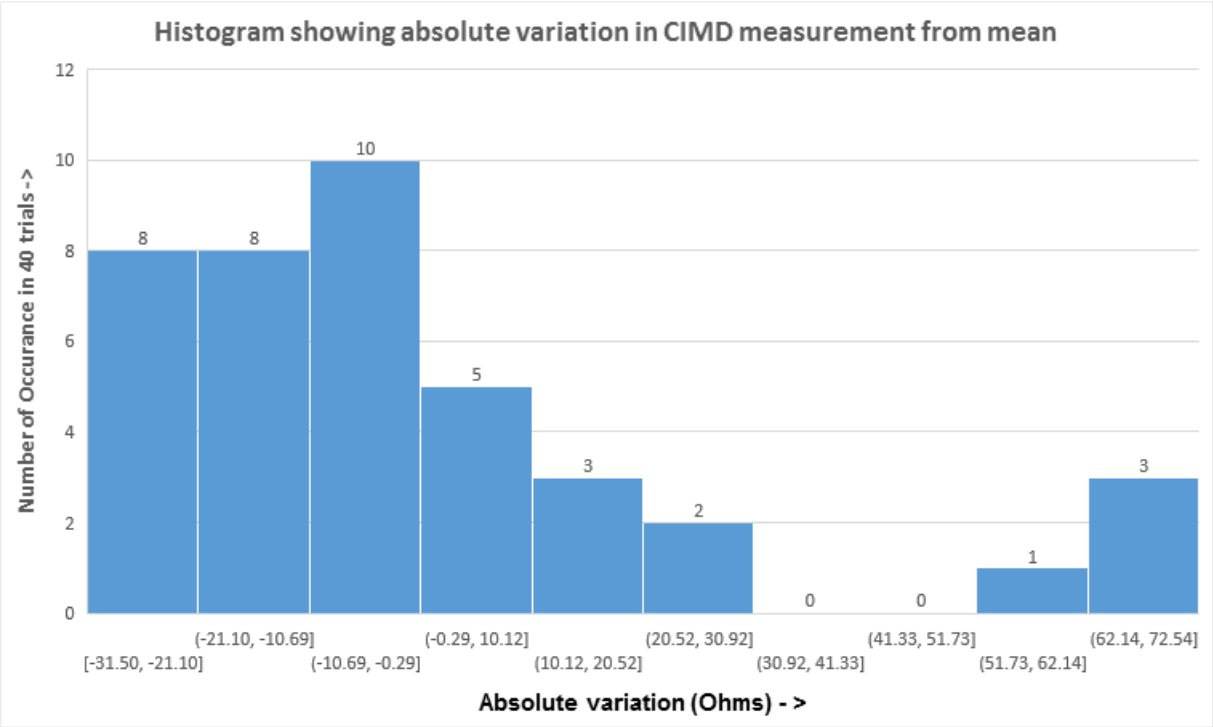

Figure 5.1. Absolute variations from mean of measurement of resistance for 40 different measurement of 18.06K Ohm calibration impedance (firmware 18K).

a standard deviation of 24.53 Ohms (0.14%). The error in measurements were calculated taking 18.06 K Ohm is the actual value of the calibration resistance. The mean of the error was 19.43 Ohm (0.1%) and the standard deviation of the error was 31.29 Ohms (0.15%). The plot showing absolute variation of the measured resistance from the mean of the measured resistance if shown in figure 5.2. This plot is indication of the precision of the device. If all the values in the plot were zero, it is a perfectly precise device. We could see that the accuracy of the device improved from 0.4% error to 0.1% error with adjusting the calibration impedance value from 18K to the actual value of 18.06 K Ohm in firmware. This is significant improvement given that the percentage standard deviation of the measured values (indication of precision) almost remained constant. It changed from 0.15% to 0.14% which is only a slight improvement when compared to the improvement in accuracy. This indicates the high importance of knowing the value of the calibration impedance to as much

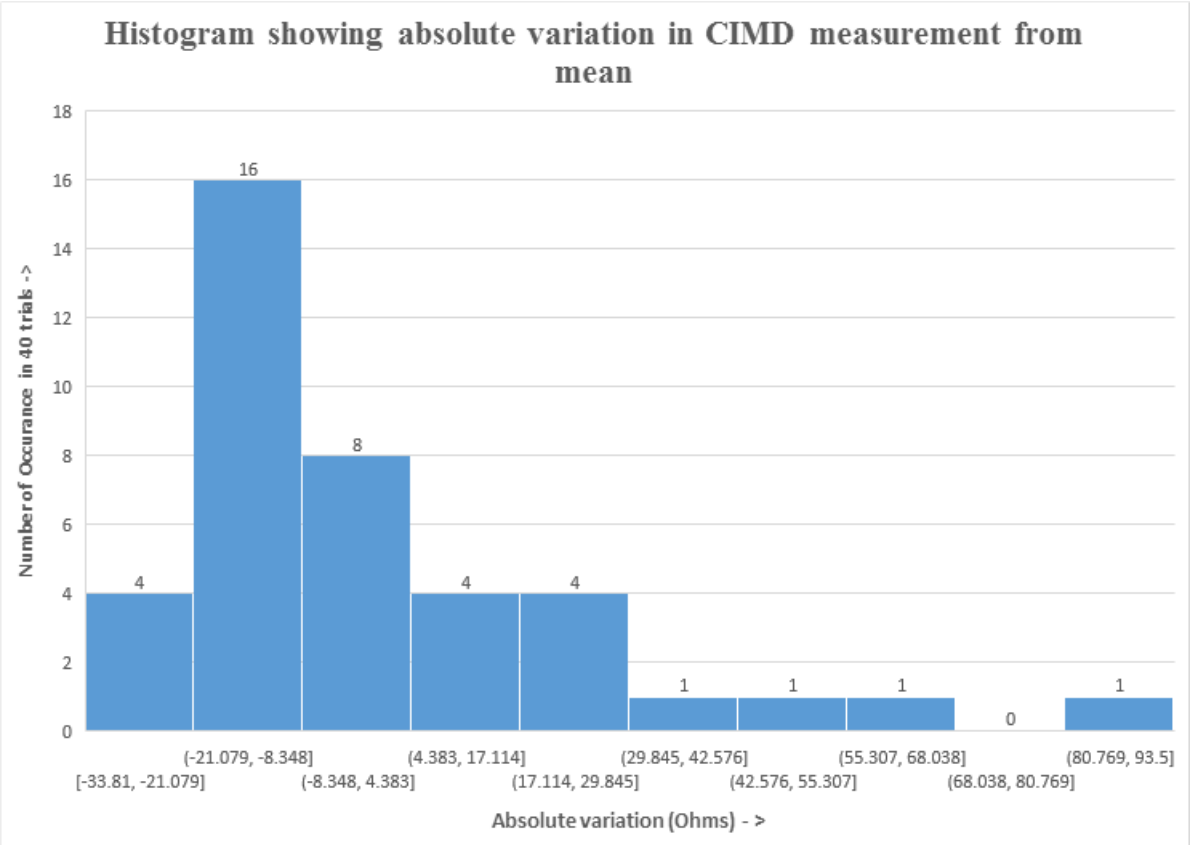

Figure 5.2. Absolute variation from mean of measurement of resistance for 40 different measurement of the 18.06K Ohm calibration impedance (firmware 18.06K).

accuracy as possible. It would be ideal to also have the calibration impedance to not change its resistance with ageing. Figure 5.3 shows the value measured by CIMD for the calibration impedance and the actual value of an 18.06K Ohm.

5.2 Resistance measurement test

The device needs to be able to measure 8K Ohm to 20KOhm impedance for being able to measure glucose from sweat. Before measuring complex impedance, simple resistance was measured and its accuracy is determined. Resistance from 5K Ohm to 30K Ohm was measured using CIMD and is compared against a digital multimeter. Off shelf resistors of 1% tolerance was used as test resistors for this test. The calibration impedance value used

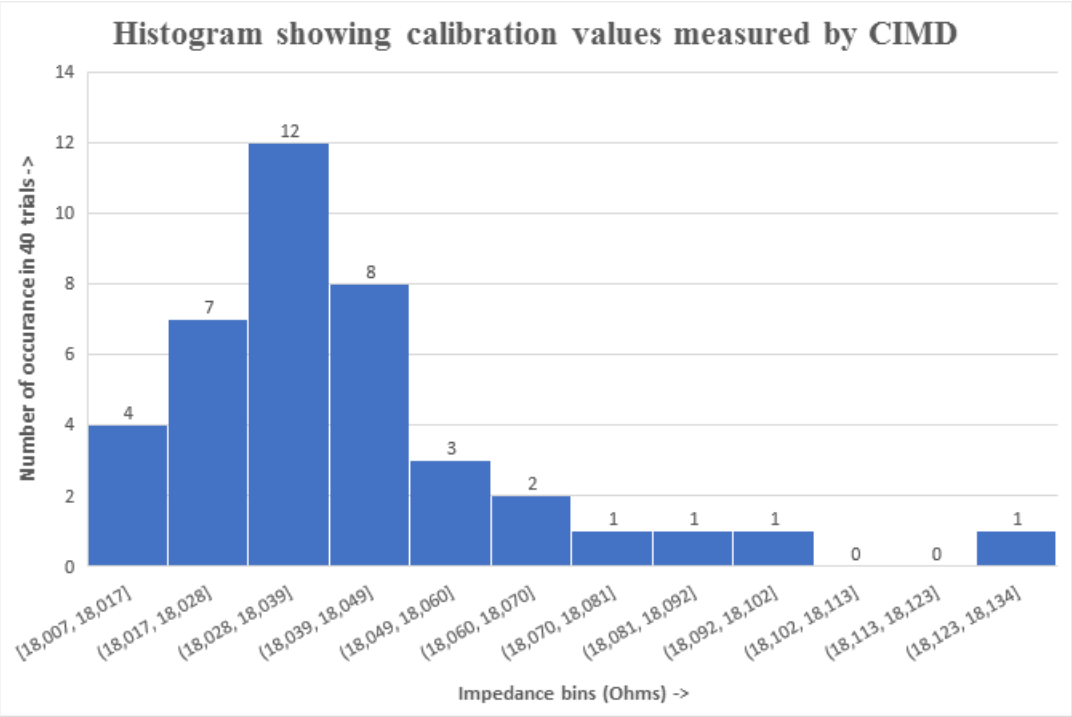

Figure 5.3. Plot showing values measured by CIMD for an 18.06K Ohm calibration impedance.

in the CIMD FCM is 18K Ohm. Twenty readings of each of the test resistor was taken. It is seen that for the required measurement range the error percentage is less than 0.5% of the test. The figure 5.4 shows the percentage error for all the measured impedances. The error percentage is seen to increase as the test resistor has higher resistance. This implies that there is significant increase in measurement error as the resistance increase. If the absolute error in resistance measurement was relatively constant over the entire range, the percent error at higher resistance should be lower than that of smaller resistance. We expect the absolute error to remain constant if the voltage input to the sampling ADC due to current signal through the impedance is within the linear region of the ADC. However, we see that the error increases with increase in resistance. This could be because the effect of noise becomes more prominent as the impedance value increases. Larger resistors have higher

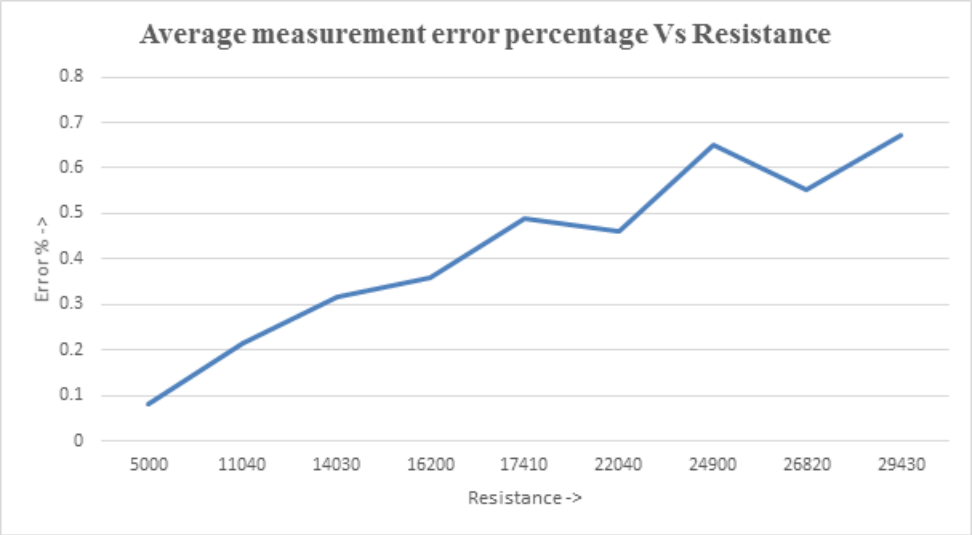

Figure 5.4. CIMD measurement error percentage for test resistances from 5K Ohm to 30K Ohm.

thermal noise associated with it. The device was calibrated using a value 18.06 K Ohm and firmware had 18K Ohm as the value. This is also the reason for increase in error

5.3 Model complex impedance measurements

The data initial dataset provided by Ms. Rujuta et al. [4] was analyzed to find the range of impedances that need to be measured across all concentrations and baseline sensor reading. The table 5.1 shows the four boundary cases within which, the complex sensor impedance value lies. The four corner cases were built using off-shelf resistors and capacitors and these were measured using Gamry 600 and using the CIMD at 100Hz and the measurement accuracy was determined. At 100Hz, the smallest real part of impedance was 8.37K Ohm and imaginary part was 2.54 K Ohm. The largest value of the real part was 19.72K Ohm and that of the imaginary part was 4.56K Ohm. The created models did not exactly match the corner cases in it imaginary part of impedance due to high tolerances of the capacitors used to build the models. The measurement results are shown in table 5.2 and it is seen that the maximum error lies under 5% for $|Z|$ and 3 degrees for phase(°).

Table 5.1. The corner cases of impedance and its physical equivalent for sensor data

Sl	case	Impedance	Series Model@ 100Hz	Implemented (Gamry measured)
1	LL	8.37 - j2.54	8.37 K Ohm, 627nF	8.62K - j17.40
2	LH	8.37 - j4.56	8.37 K Ohm, 81nF	8.56K - j2.73K
3	HL	19.72 - j2.54	19.72 K Ohm, 627nF	19.68K - j2.69K
4	HH	19.72 - j4.56	19.72 K Ohm, 81nF	19.60K - j2.74K

Table 5.2. Measurement results of Gamry and CIMD, showing the error percentage in CIMD measurement.

Sl	Case	Gamry $\mid Z \mid$	Gamry(°)	CIMD $\mid Z \mid$	CIMD(°)	$\mid Z \mid$ error%	(°) error %
1	LL	19429.06	-63.63	20222.86	-65.42	4.08	1.79
2	LH	8996.48	-17.25	9019.01	-18.77	0.25	0.92
3	HL	26473.21	-41.11	27010.62	-43.86	2.03	2.74
4	HH	19799.90	-7.97	19842.35	-8.77	0.21	0.79

5.4 Glucose sensor measurements

The glucose sensor that is used to test glucose from sweat is in its developmental research phase. In its current condition, it does not have a fixed baseline impedance value. The value increases with time due to drying up of the baseline solution. The rate of drying is dependent on the environmental conditions like temperature, humidity and the voltage signals applied to the sensor. No signal is applied to the sensor (sensor is kept floating) to remove the dependence of the applied signal. It is necessary to perform the measurement after a constant time interval after the solution has been added to have a consistent snapshot of the sensor. The time interval should be large enough for the reactions going on in the sensor to reach equilibrium. By ensuring a constant time interval before the measurement is done, the state of the sensor should very close every time a sensor is used. This time interval is called the incubation time. If we configure the measurement devices to measure multiples times, the measurement of impedance of the sensor cannot be done, one after the other using Gamry and CIMD because the value of impedance will change by the time the first device has completed measurements. The options to eliminate this problem is to either take one sample using a device and the next using the other device and find out if they

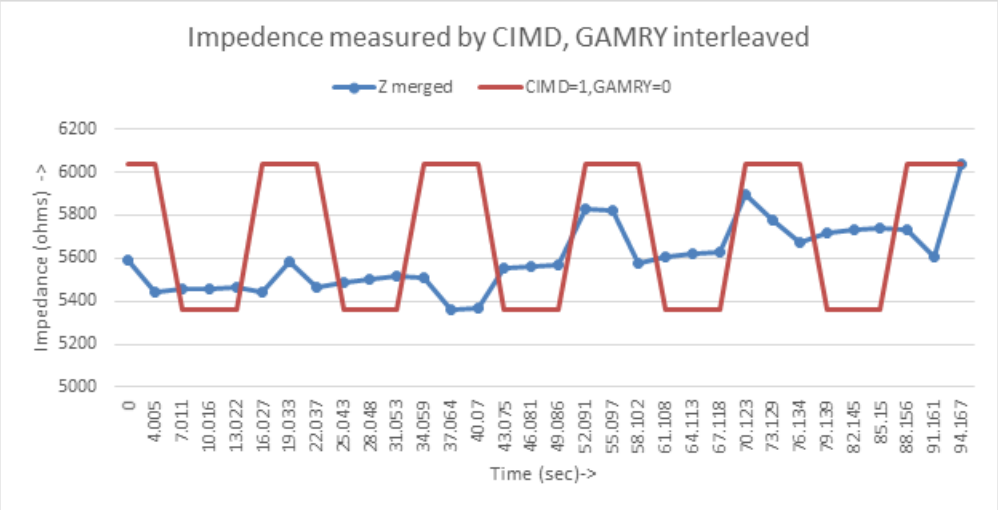

follow each other or to just take a single or very few measurements as fast as possible and measure it using the next device. The figure 5.5 shows measurement of baseline impedance magnitude using CIMD and Gamry alternatively, after each device measures three samples. This was achieved by using an MUX external to both the measurement devices. The sensor channel was connected to one of the two devices at a time, while both the devices continuously performed measurements. We could see that the measurements follow almost the same increasing trend in both devices. However, this was not seen once the sensor was spiked with glucose doses. This is because of the effect of the transient currents influencing the senor behavior in the presence of glucose.

The next alternative is to do a single or very few measurements using one device followed by the other device without giving much time in between the devices. This gave us measurements with good accuracy for CIMD with respect to the Gamry measurements. Figure 5.6 shows the measurement results for a sensor measured using both devices. It can be seen that the CIMD measured values are very close to the one measured by Gamry. The percentage error in measurement of impedance is given in figure 5.7. The $|Z|$ error percentage was less than 2.5% and phase error less than 1.5% for this sensor sample. This is the results of one

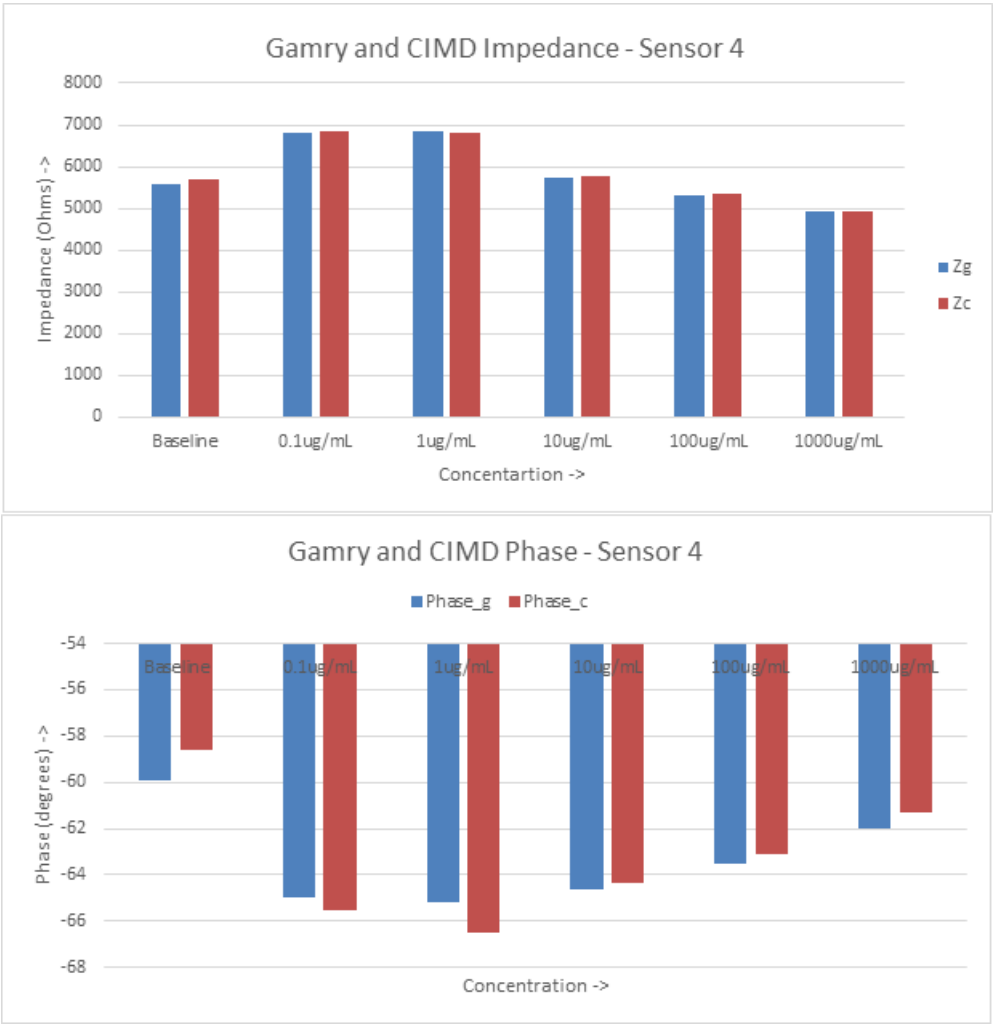

Figure 5.6. Gamry and CIMD measurements for various concentration for a glucose sensor showing magnitude and phase of measurements - Gamry (blue), CIMD (red).

among the three sensors (sensor 1, sensor 2, sensor 4) that was tested this method. Sensor 1 and sensor2 gave similar results as shown in figure 5.6 and 5.7. One of the sensor however, had a larger error percentage in measurement. The baseline impedance measurement was the most affected measurement in this sensor and thus, the error percentages were up to 8% was seen for the glucose test samples but phase error was within 1.5%. The measured impedances in the three sensors for different concentrations of glucose were used to find the percentage change in impedance from their respective baseline sensor impedance. This was done using

Figure 5.7. Impedance magnitude error percentage and phase error in degrees for various concentration of glucose.

both Gamry and CIMD using their respective baseline measurements. Four sensors were intended to be tested but the sensor 3 was not tested in CIMD as it was had manufacturing defects. It showed mismatch from expected impedances values even before it reached the final stage of manufacturing. We can see that the percentage change in senor 1 and sensor 4 are closely matching the in both the instruments. This shows that CIMD can be used to accurately measure impedance of the glucose sensor and calculate glucose concentration with it. The baseline measurement in sensor 2 using CIMD was erroneous hence there is a larger error in percentage change is seen in with respect to Gamry in figure 5.8. A larger value of baseline impedance was seen than expected in CIMD measurements. The average of three measured values were used as the reported value. Three sample measurements were performed by CIMD and the initial two readings were close to that of Gamry reading while the third reading had a significant increase (erroneous measurement) resulting in an increase

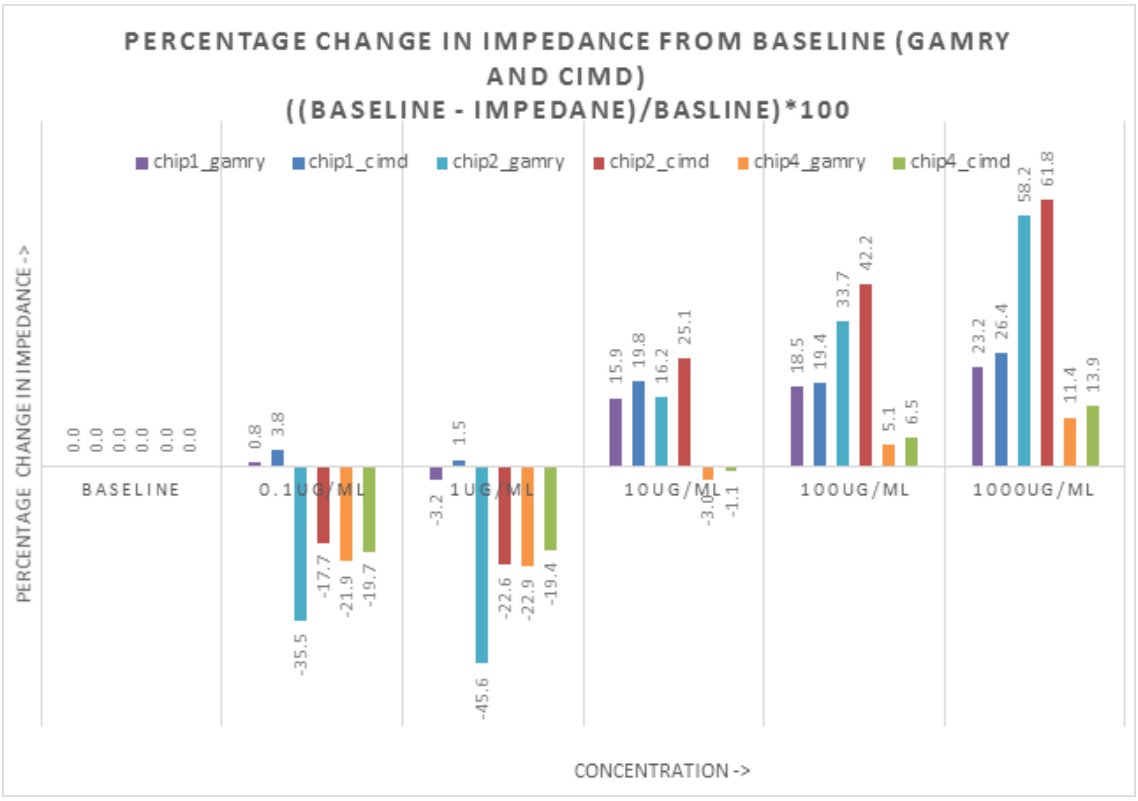

Figure 5.8. Percentage change in impedance from baseline for varying concentrations of glucose in test samples. Both Gamry and CIMD results are shown adjacent to each other for the three sensors that were tested.

in reported impedance value. There error could also be due to any number of factors like noise, motion artifacts etc. but the definite reason is not known. If we correct the baseline measurement of sensor 2 to match Gamry, we can see that the percentage changes of sensor 2 using CIMD match with expected accuracy (less than 4%) to that of Gamry as shown in figure 5.9. We see that by correcting the erroneous baseline value measurement we can see that the error in percentage changes decreased to the less than 4% for relevant concentrations (10ug/ml, 100ug/ml and 1000ug/ml) as seen in other sensor measurements.

We observe that percentage change decreased (indicating an increase in impedance) from baseline for 0.1ug/ml and 1ug/ml concentrations for all three sensors. We expected a decrease in impedance rather than an increase. This indicate that none the sensors responded to these concentrations of glucose. This is due to stability issues in the immunoassay used to

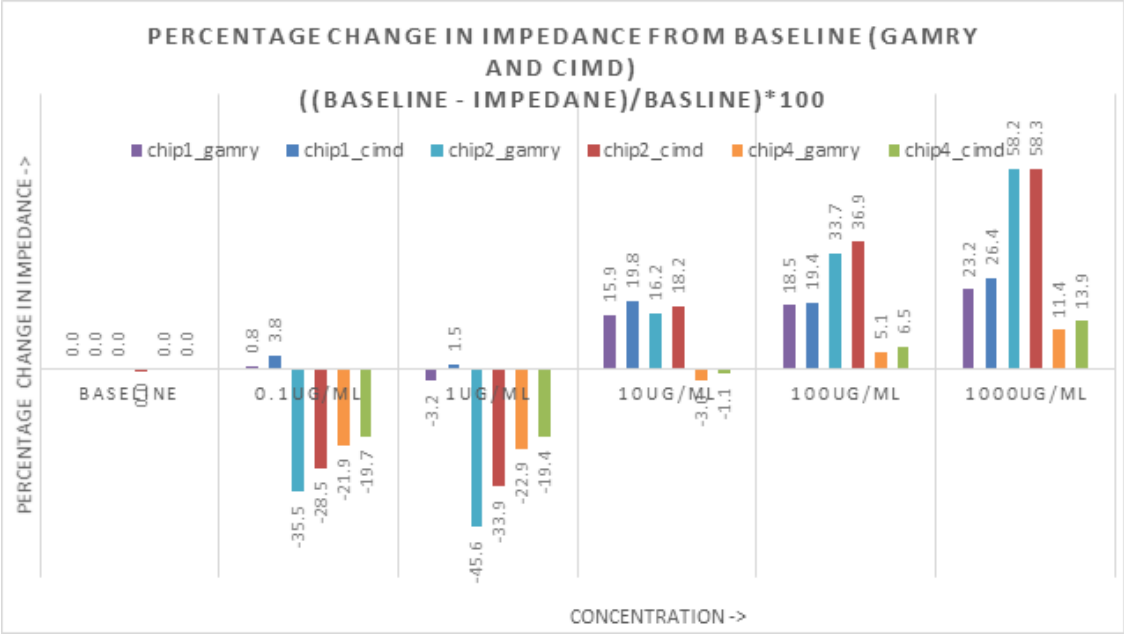

Figure 5.9. Percentage change in impedance from baseline for varying concentrations of glucose in test samples (Baseline measurement corrected for sensor 2 to match Gamry value).

prepare the sensors. Sensor 1 and 2, at higher concentrations of glucose showed a decrease in impedance; the trend that we expect from it. Sensor 1 and Sensor 4 was found to be defective sensor because it did not have the baseline impedance in the 8-20K Ohm range. We can use the percentage change in impedance at 10ug/ml, 100ug/ml and 1000ug/ml to calculate the concentration of glucose for the two sensors using the measurements for Gamry and CIMD measurements using the concentration calibration look up table shown in table 5.3 obtained from [4]. The calculated glucose concentration is shown in table 5.4 The sensor 1 and sensor 2 gave results as expected trend of decrease in impedance from baseline showing its expected functionality for concentrations 10ug/ml and 100ug/ml and 1000ug/ml (1mg/dl to 100mg/dl) which are relevant range of glucose concentration in human sweat. Gamry and CIMD could come to the same predictions for senor 1 even though it is defective (baseline impedance close to 5 K Ohm instead of being in the expected 16 to 20K ohm). Sensor 2 has same larger error due to erroneous sample in baseline. All percentage difference in impedance are calculated from the baseline impedance. A large error in baseline

Table 5.3. Calibration look up table for mapping percentage impedance change to concentration.

Percentage Change	**Concentration**
[12% - 21%]	0.1ug/ml
[21% - 25%)	1 ug/ml
[25% - 28%)	1ug/ml to 10ug/ml
[28% - 31%)	1ug/ml to 100ug/ml
[31% - 35%)	10ug/ml to 100ug/ml
[35% - 39%)	100ug/ml
[39% - 43%)	100ug/ml to 1000ug/ml
[43% - 49%)	1000ug/ml

Table 5.4. Concentration of glucose derived from measurement using Gamry and CIMD using look up table. The percentage changes used to look up the concentration is also given in table. The X indicates a percentage change out of the limits of the studies by [4].

Dose	**Sensor 1**		**Sensor 2**		**Sensor 4**	
Concentartion	**Gamry**	**CIMD**	**Gamry**	**CIMD**	**Gamry**	**CIMD**
10ug/ ml	0.1ug/ml 15.90%	0.1ug/ml 19.80%	0.1ug/ml 16.20%	1-10ug/ml 25.10%	X -3.00%	X -1.00%
100ug/ml	0.1ug/ml 18.50%	0.1ug/ml 19.40%	10-100ug/ml 33.70%	100-1000ug/ml 42.20%	X 5.10%	X 6.50%
1000ug/ml	1ug/ml 23.30%	1-10ug/ml 26.40%	1000ug/ml /x 58.20%	1000ug/ml /x 61.80%	X 11.40%	0.1ug/ml 13.90%

measurement will cause a large percentage error in all the impedance changes even if rest of the measurements is correct. The baseline corrected value is used for sensor 2 and used to calculate the glucose concentration as shown in table 5.5. With this correction in baseline value the CIMD showed less than 4% error as expected from Gamry measurements, in the percentage change in impedance from baseline.

Table 5.5. Concentration of glucose derived from measurement using Gamry and CIMD using look up table (with sensor 2 baseline error corrected). The percentage changes used to look up the concentration is also given in table.

Dose Concentartion	**Sensor 1**		**Sensor 2**		**Sensor 4**	
	Gamry	**CIMD**	**Gamry**	**CIMD**	**Gamry**	**CIMD**
10ug/ ml	0.1ug/ml 15.90%	0.1ug/ml 19.80%	0.1ug/ml 16.20%	0.1ug/ml 19.80%	X -3.00%	X -1.00%
100ug/ml	0.1ug/ml 18.50%	0.1ug/ml 19.40%	10-100ug/ml 33.70%	100ug/ml 36.90%	X 5.10%	X 6.50%
1000ug/ml	1ug/ml 23.30%	1-10ug/ml 26.40%	1000ug/ml /x 58.20%	1000ug/ml /x 58.30%	X 11.40%	0.1ug/ml 13.90%

CHAPTER 6

CONCLUSION AND FUTURE WORK

This chapter briefly goes through the results and conclusion of this work. It also discusses the future scope of the work. The work aimed at building a proof of concept device that is portable and configurable, used a to detect a disease using nanosensor tailored for detecting a specific molecule. The device is built to interface with any two-electrode electrochemical impedance spectroscopy (EIS) sensor that works within the operational limits of this device. It is tested with the sweat based glucose sensor developed by Rujuta et al. [4]. This sensor along with the developed device can be used to non-invasively to test for diabetes. Even though the sensor has high variability in baseline sensor impedance, the sensor gives detectable change in impedance for the range of glucose concentration relevant to human sweat with very little volume of 3 micro liters of sweat. Once the sensor technology become more robust it has the potential to replace the blood based glucose testing and the developed device could be used with it. The complete system is built on a flexible architecture that allows for configuring the device for a different sensor or even for different sensing technique. The device consists of a fixed configurable module made up of an Arduino prototyping platform and a technique specific reusable module which is a custom-built board called configurable impedance measurement device (CIMD) which can measure complex impedance. These two boards are interfaced using a standard I2C bus. The device can generate sinusoids from amplitude 2mV to 3V and 1Hz to 2MHz frequency using the impedance convertor device (AD5933) which has a recommended maximum operating frequency of 100KHz and gives only four discrete amplitude choices. Measurement above 100KHz require multipoint calibration to account for the change in gain of the AD5933 internal low pass filter. As the frequency is increased from 100 KHz the measurement accuracy will go down even if multipoint calibration is done, due to loss of signal amplitude.

6.1 Conclusion

The developed device (CIMD) could measure impedances in the required range of 8 to 20K Ohm and it was used to measure the impedance of the sensor with baseline solution and with varying doses of glucose it. The percentage change in impedance from the baseline impedance were used to calculate the dose of glucose in the test sample. The measurements done for the glucose in CIMD agree with Gamry 600 measurement device with maximum error percentage of 0.4Before measuring in the glucose sensor, model complex impedances were built using off shelf resistors and capacitors and tested with CIMD and Gamry and it gave a maximum error percentage less than 4.5% in impedance magnitude. Also, resistors from 5 to 30K Ohm were measured for its resistance and it gave less than 1% error with respect to a digital multimeter reading and gave error less than 0.5% for the required impedance range of 8 to 20K Ohm. The amplitude of the sinusoid generated can be controlled either by a gain setting resistor (R2) or setting the value of a digital potentiostat (U12) in figure 4.1. In a similar fashion the range of impedance that can be measured can be adjusted by a different gain setting fixed resistor (R5) or a digital potentiostat (U3) in figure 4.1. The device can be configured to be tested for a different range of impedances either by replacing two resistors (gain setting resistors) with different values of resistors or by changing the digital potentiostat values that does the same function.

Changing the fixed resistors (hardware) would give more accurate results when compared to changing the digital potentiometer values (firmware change). The sinusoid that is applied at the sensor is seen to be noisy if the digital potentiostat is used in the signal chain instead of the fixed resistors. This problem can be fixed if a programable band pass filter can be used at the output of digital potentiometer. This is however not implemented in the current CIMD system. The device should be able to accurately measure impedances from 10 Ohm to 2 Mega Ohm which spans the entire range of impedances that the AD5933 datasheet

Table 6.1. Comparison of the CIMD with existing device in literature [10] with CIMD included in table

Author	**Purpose**	**Frequency Range**	**Impedance Range**	**Maximum $\mid Z \mid$ error (%)**	**Maximum Phase error(°)**
C.J Chen et al. [11]	Cell culture monitoring	Fixed 10Hz	No data	No data	
T.Schwarzenberger et al. [12]	Cell culture monitoring	100Hz - 100KHz	No data	2% - modulus	2% - argument
M.H Wang et al.[13](AD5934 used)	Single cell measurement	0.1Hz - 100KHz	100 -10 M	Over 10% for cell measurement	No data
J. Broeders et al. [14]	Biosensor applications	10Hz - 100KHz	10 to 5 M	No data	No data
P.Bogonez-Franco et al. [15]	Bioimpedance Monitor	100Hz - 200KHz	10 to 1K	2.5% - modulus	4.5% - argument
J. Ferreira et al. [16]	Bioimpedance with Textile electrodes	5KHz 450KHz	No data	0.7% - reistance	17% - reactance
C. Margo et al. [17]	Bioimpedance Embedded application	1KHz 100KHz	No data	2.5% - modulus	1.3% - argument
A Melwin and K. Rajasekaran [18]	Body composition Measurement	Fixed 50KHz	No data	2% (not specified)	
J. Hoja and G. Lentka [19 20]	Technical objects Monitoring	0.01 Hz 100KHz	10 10G	1.6% -modulus	0.6% -argument
CIMD	Biosensor application	1Hz 2MHz	5K 22K	0.5% - resistor 4% - impedance	0.41% - argument

Note: CIMD accuracy based on single frequency measurements at 100Hz.

specifies that it can measure with accuracy. This can be achieved using appropriate gain setting resistors.

6.2 Future scope

There are several improvements that can be done on the CIMD board as future directions that could make the system perform better. The first the board could be modified to add programmable band pass filter at the digital potentiometer output to make the signal chain including the digital potentiometer less noisy. This would enable us to program the board to automatically configure its gain settings to accurately measure the impedances. An auto ranging function to automatically select calibration resistance can also be implemented in firmware. The effect of noise can be reduced by implementing techniques like faraday shielding to improve accuracy of measurements. Detailed studies on the effect of different gain configuration, clock frequency and settling time can be done and statistical analysis performed to find an algorithm to choose the best configuration to measure an impedance range. The two methods of improving range of measurements, either using multiple fixed resistors or using low noise digital potentiometers with band pass filers can be implemented to find out which implementation results in more accurate results.

The overall system functionality can be improved by making the device wireless. This can be done with no modification in CIMD hardware or the FCM firmware. The FCM can be replaced to an Arduino BT to enable wireless communication between the host PC and the board.

A mobile application can be developed that can be used to configure the FCM device for different sensors. These changes can make sufficient performance improvement in terms of accuracy over a large range of impedances and frequency. The system made more user-friendly and versatile using a smartphone application that can configure the FCM.

Another direction in the future scope, would be to make the device smaller by using smaller

footprint components. The power utilization can be studied and better power management can be implemented to make the device operate on battery for considerable amount of time.

REFERENCES

[1] Rujuta D Munje, Sriram Muthukumar, Anjan Panneer Selvam, and Shalini Prasad. Flexible nanoporous tunable electrical double layer biosensors for sweat diagnostics. *Scientific reports*, 5, 2015.

[2] James Moyer, Donald Wilson, Irina Finkelshtein, Bruce Wong, and Russell Potts. Correlation between sweat glucose and blood glucose in subjects with diabetes. *Diabetes technology & therapeutics*, 14(5):398–402, 2012.

[3] Alexander Sun, Travis Wambach, AG Venkatesh, and Drew A Hall. A multitechnique reconfigurable electrochemical biosensor for integration into mobile technologies. In *Biomedical Circuits and Systems Conference (BioCAS), 2015 IEEE*, pages 1–4. IEEE, 2015.

[4] Rujuta D Munje, Sriram Muthukumar, and Shalini Prasad. Lancet-free and label-free diagnostics of glucose in sweat using zinc oxide based flexible bioelectronics. *Sensors and Actuators B: Chemical*, 238:482–490, 2017.

[5] MGVV Bothara, V Venkatraman, R KK Reddy, T Barrett, J Carruthers, and S Prasad. Nanomonitors: electrical immunoassays for protein biomarker profiling. 2008.

[6] Byoung-Yong Chang and Su-Moon Park. Electrochemical impedance spectroscopy. *Annual Review of Analytical Chemistry*, 3:207–229, 2010.

[7] Analog Devices. Datasheet and Product Info — Analog Devices. `http://www.analog.com/en/products/rf-microwave/direct-digital-synthesis/ad5933.html`, 2016. [Online; accessed 27-November-2016].

[8] Rajesh Kannan Megalingam, Goutham Pocklassery, Athul Asokan Thulasi, Vivek Jayakrishnan, and Galla Mourya. Medisuit: Wearable health monitoring system for elders and bed-ridden patients. In *Intelligent Systems and Control (ISCO), 2016 10th International Conference on*, pages 1–6. IEEE, 2016.

[9] Google ATAP. Project Jacquard. `https://atap.google.com/jacquard/`, 2016. [Online; accessed 27-November-2016].

[10] Konrad Chabowski, Tomasz Piasecki, Andrzej Dzierka, and Karol Nitsch. Simple wide frequency range impedance meter based on ad5933 integrated circuit. *Metrology and Measurement Systems*, 22(1):13–24, 2015.

[11] Ching Jung Chen, Jen Tsai Liu, Shwu-Jen Chang, Ming-Wei Lee, and Jang-Zern Tsai. Development of a portable impedance detection system for monitoring the growth of mouse l929 cells. *Journal of the Taiwan Institute of Chemical Engineers*, 43(5):678–684, 2012.

[12] T Schwarzenberger, P Wolf, M Brischwein, R Kleinhans, F Demmel, A Lechner, B Becker, and B Wolf. Impedance sensor technology for cell-based assays in the framework of a high-content screening system. *Physiological measurement*, 32(7):977, 2011.

[13] Min-Haw Wang, Min-Feng Kao, and Ling-Sheng Jang. Single hela and mcf-7 cell measurement using minimized impedance spectroscopy and microfluidic device. *Review of Scientific Instruments*, 82(6):064302, 2011.

[14] Jeroen Broeders, Stijn Duchateau, Bart Van Grinsven, Wouter Vanaken, Marloes Peeters, Thomas Cleij, Ronald Thoelen, Patrick Wagner, and Ward De Ceuninck. Miniaturised eight-channel impedance spectroscopy unit as sensor platform for biosensor applications. *physica status solidi (a)*, 208(6):1357–1363, 2011.

[15] P Bogónez-Franco, Antoni Bayés-Genís, J Rosell, and R Bragós. Performance of an implantable impedance spectroscopy monitor using zigbee. In *Journal of Physics: Conference Series*, volume 224, page 012163. IOP Publishing, 2010.

[16] Javier Ferreira, Fernando Seoane, and Kaj Lindecrantz. Ad5933-based electrical bioimpedance spectrometer. towards textile-enabled applications. In *2011 Annual International Conference of the IEEE Engineering in Medicine and Biology Society*, pages 3282–3285. IEEE, 2011.

[17] C Margo, J Katrib, Mustapha Nadi, and Amar Rouane. A four-electrode low frequency impedance spectroscopy measurement system using the ad5933 measurement chip. *Physiological measurement*, 34(4):391, 2013.

[18] Guo Bing Huang, Hua Li Li, and Rui Ling Li. Implementation of alternating analog input board on arm7. In *Advanced Materials Research*, volume 823, pages 532–535. Trans Tech Publ, 2013.

[19] Jerzy Hoja and Grzegorz Lentka. Interface circuit for impedance sensors using two specialized single-chip microsystems. *Sensors and Actuators A: Physical*, 163(1):191–197, 2010.

[20] Jerzy Hoja and Grzegorz Lentka. A family of new generation miniaturized impedance analyzers for technical object diagnostics. *Metrology and Measurement Systems*, 20(1): 43–52, 2013.

[21] Analog Devices. Evaluation Board — Analog Devices. `http://www.analog.com/en/design-center/evaluation-hardware-and-software/evaluation-boards-kits/eval-ad5933.html`, 2016. [Online; accessed 27-November-2016].

[22] DK Kamat, Dhanashri Bagul, and PM Patil. Blood glucose measurement using bioimpedance technique. *Advances in Electronics*, 2014, 2014.

[23] Aaron A Rowe, Andrew J Bonham, Ryan J White, Michael P Zimmer, Ramsin J Yadgar, Tony M Hobza, Jim W Honea, Ilan Ben-Yaacov, and Kevin W Plaxco. Cheapstat: An open-source,do-it-yourself potentiostat for analytical and educational applications. *PloS one*, 6(9):e23783, 2011.

[24] Gamry. Potentiostat Fundamentals. `http://www.gamry.com/application-notes/instrumentation/potentiostat-fundamentals/`, 2016. [Online; accessed 27-November-2016].

[25] Wei Gao, Sam Emaminejad, Hnin Yin Yin Nyein, Samyuktha Challa, Kevin Chen, Austin Peck, Hossain M Fahad, Hiroki Ota, Hiroshi Shiraki, Daisuke Kiriya, et al. Fully integrated wearable sensor arrays for multiplexed in situ perspiration analysis. *Nature*, 529(7587):509–514, 2016.

[26] Oscar Olarte, José Chilo, José Pelegri-Sebastia, Kurt Barbé, and Wendy Van Moer. Glucose detection in human sweat using an electronic nose. In *2013 35th Annual International Conference of the IEEE Engineering in Medicine and Biology Society (EMBC)*, pages 1462–1465. IEEE, 2013.

VITA

Athul Asokan Thulasi was born in Kalpetta, Kerala, India on May 1992. He finished his high school in 2010 from Kendriya Vidyalaya, Kalpetta. After that, he completed his undergraduate degree (B.Tech) in Electronics and Communication with distinction from Amrita University, India in 2014. He joined The University of Texas at Dallas for his Masters of Science(M.S) in Electrical Engineering in 2014. He had interned in Xilinx Inc. during in summer of 2016 in the evaluation boards team, while he was pursuing his graduate studies. His research interest includes reconfigurable computing, product development and biomedical devices.